Journal of Power Sources 450 (2020) 227632

Contents lists available at ScienceDirect

Journal of Power Sources

journal homepage: www.elsevier.com/locate/jpowsour

Review article

Protective coatings for lithium metal anodes: Recent progress and future perspectives

Hongyao Zhou, Sicen Yu, Haodong Liu **, Ping Liu *

Department of NanoEngineering, University of California San Diego, 9500 Gilman Drive, La Jolla, CA, 92093, USA

HIGHLIGHTS

- This review covers recent advancements in protective coatings for Li metal anode.
- The design criteria for an effective coating are proposed.
- Ion conduction mechanisms of inorganic and polymeric coatings are discussed.
- Demonstration of the protective function in realistic cell condition is advocated.

ARTICLE INFO

Keywords:
Lithium batteries
Lithium metal anode
Protective layer
Ion conduction mechanism

ABSTRACT

The demand for lithium batteries with energy densities beyond those of lithium-ion has driven the recent studies on lithium metal anode. High-efficiency electrochemical cycling of lithium requires improved lithium deposition morphology and reduced parasitic reactions between lithium and the liquid electrolyte. A protective layer on lithium metal is expected to reduce contact between lithium metal and the organic solvent, exert compressive mechanical force on the anode, and improve the selectivity and uniformity of lithium ion transport at the electrode surface. This review covers recent advancements in this topic. We first establish the design criteria for an effective coating followed by a brief description of the methods for depositing the layer, characterizing its structure and morphology, and evaluating its electrochemical performance. Our discussion of the literature is organized on resultant layer composition and corresponding ion conduction mechanisms. In the case of polymeric materials, the polarity difference between the polymer and electrolyte solvents determines the degree of swelling and selectivity of lithium ion transport. We conclude by advocating for the need of increased mechanistic study for the functioning mechanism, improved understanding of layer degradation, and demonstration of the protective function in realistic cell environment, namely lean electrolytes and coupled with appropriate cathodes.

1. Introduction

Booming popularity of electric vehicles requires batteries to increase the energy density to more than 500 Wh kg^{-1} [1]. Conventional Lithium (Li)-ion battery has achieved excellent cycling performance through the intercalation chemistries, however, the low theoretical capacity of graphite anode limits the energy density of the battery. Li metal anode uses reversible electroplating and stripping of metallic Li to store energy [2]. The theoretical capacity of Li metal anode (3860 mAh g^{-1}) is ten times higher than the value of graphite (372 mAh g^{-1}). Therefore, Li metal is regarded as the anode for next-generation high energy density Li batteries. Li metal anode is widely studied for the application in both liquid-electrolyte-based and all-solid-state batteries. Advantages of liquid-electrolyte-based Li metal battery are the fast ion transport at the electrode-electrolyte interface, and the mature battery mass production process. Recently, liquid electrolyte based Li metal battery with an energy density of 300 Wh kg^{-1} and 86% capacity retention for 200 cycles is reported [3]. However, the cycling life still needs to be improved for practical applications.

Failure of Li metal battery often stems from the Li anode side: The Li metal foil, initially of a shiny metallic color, turns black after several cycles, because the Li metal forms a microporous and mossy structure

* Corresponding author.
** Corresponding author.
E-mail addresses: haodong.liu.xmu@gmail.com (H. Liu), piliu@eng.ucsd.edu (P. Liu).

https://doi.org/10.1016/j.jpowsour.2019.227632
Received 16 November 2019; Received in revised form 14 December 2019; Accepted 16 December 2019
Available online 23 December 2019
0378-7753/

(Fig. 1a) [3,4]. The surface of this mossy Li metal is covered with a passivation (solid electrolyte interface, SEI) layer, and isolation of these Li microparticle from the current collector (formation of "dead Li") results in loss of anode capacity [5]. Furthermore, the porous Li metal with high surface area promotes the side reactions and quickly consumes the liquid electrolyte, which results in increased cell impedance.

Several strategies have been reported to improve the cycle life of Li metal anode, primarily based on the hypotheses of minimizing reactions between lithium metal and the electrolyte, and maintaining electric contact between deposited lithium metal particles. These approaches include: 1) electrolytes with low chemical reactivity with Li metal, for example using highly concentrated salt or fluorinated solvent [6–8]; 2) additives to passivate the surface of Li metal and regulate the morphology [9,10]; 3) surface modifications of the polymer separator [11,12]; 4) current collectors with 3D framework to guide the deposition of Li metal [13–16]; 5) surface pretreatments of Li metal or the current collector with a protective coating to stabilize the interface between Li metal and electrolyte (focus of this review); 6) high external pressure to promote flat depositions of Li metal [17,18].

Protective coatings are ion-conductive or electrolyte-permeable layers underneath which Li metal can be electrodeposited (Fig. 1b). As Li ions pass through the coating layer, the ion flux becomes more homogeneous at the electrode surface, leading to uniform Li metal deposition [19,20]. The protective layer also reduces the contact area between the electrolyte and Li, thus suppresses the side reactions. In contrast to SEI layer formed by the side reaction inside the battery, protective coatings for Li metal can be viewed as a preformed, artificial SEI layer. The composition of the coating materials can be tuned to optimize the ionic conductivity, the mechanical strength, and the permeability to the solvent [21,22].

Previously, protective coatings were reviewed as one approach to stabilize the electrolyte-Li metal interface, as reported by Archer, Cui, Zhang et al., respectively [2,20,23,24]. More recently, a comprehensive review covering the interface engineering at Li metal anode was published by Zhang et al. [25] These reviews provide excellent and extensive summaries of synthesis approaches for protective coatings, and descriptions of how different coatings improve lithium metal anode cycling performance.

The continuous publication of a large number of peer-reviewed studies on the protective coating motivated us to focus our review on works published from 2017 to 2019. We chose references reporting the results of Li||Li symmetric cycling, Cu||Li CE test, Li||cathode cell test with well-described testing conditions (discussed in Section 5) to allow precise comparisons among different coating materials. Instead of providing a comprehensive account of published literature, this review attempts to analyze reported literature based on how different coating materials accomplish both protective and ion-conducting functions simultaneously and the intrinsic tradeoff between them. We hypothesize that the protection mechanism of coatings to be: 1) mechanical suppression of dendritic Li; 2) reduced side reaction by chemical selectivity.

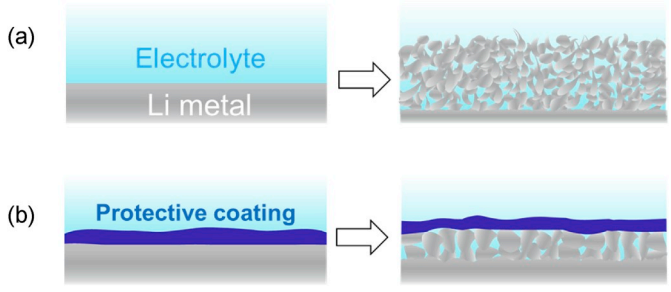

Fig. 1. (a) Porous morphology of electroplated Li metal after long period of cycling. (b) Dense morphology of Li metal electroplated underneath the protective coating. The coating also protects Li metal from side reactions with the electrolyte.

In addition to these two protection mechanisms, ionic conductivity is an essential feature of the coating, because Li ion is required to transport through the layer.

This review is organized as the following: proposal of the functioning mechanisms of the coating layer based on previous studies of interfacial physics and chemistry between Li metal and the electrolyte (Section 2), review of various techniques for the preparation of coating layers (Section 3), the characterization techniques of the coatings (Section 4), and the performance evaluation of the coatings (Section 5). The protective coatings are divided into inorganic materials (Section 6) and polymeric materials (Section 7), and the material properties and the stabilization effect on Li metal are discussed in detail. Composite coatings of inorganic and polymer materials are also discussed in Section 7. Based on the reported results and discussions, we provide guidelines for designing effective coating layers and suggest testing protocols to rigorously evaluate the performance of protective coatings on Li metal under practical cell conditions (Section 8).

2. Protection mechanism and key requirements for the coating layers

Protection mechanism of coating layers on Li metal can be categorized into two types: mechanical suppression of Li dendrite, and high selectivity toward Li-ion transport. For the mechanical suppression, a theoretical calculation by Newman et al. showed that compressive forces on the Li metal surface can promote Li deposition at the concave area, if the surface layer has more than two-times higher shear modulus than Li metal (Fig. 2a) [26,27]. This theory supports the basic idea of using hard inorganic materials to suppress the dendritic growth of Li metal. For example, a ceramic solid ion conductor, $Li_7La_3Zr_2O_{12}$ (LLZO), has the shear modulus of 56–61 GPa, one order of magnitude higher than the value of Li metal (4.25 GPa) to effectively suppress the Li dendrites [28].

Unlike inorganic materials, the shear modulus of organic polymer materials (e.g. 26.2 MPa for PEO [29]) are significantly lower than the value of Li metal to validate the Newman model. Srinivasan modified the Newman model by taking into account for the plastic deformation of Li metal under a high mechanical pressures [30]. The authors showed that increasing yield strength of the polymer layer (i.e. lower elasticity) promotes plastic deformation of Li metal and hence suppresses Li dendrite. In contrast, Archer et al. showed increasing viscoelasticity of electrolytes suppresses the Li dendrite growth based on the theory of electro-convection [31,32]. This theory supports the stabilization effect of Li metal by soft and gel-like polymer coatings [33,34].

Selective Li-ion transport means the coating layer selectively conducts Li ion while expelling solvent or anion molecules from Li metal surface (Fig. 2b). Li ion is always solvated by solvent molecules or anions [35–37], and the contact between the Li metal and solvent molecules/anions is inevitable during the electrodeposition. The contact between liquid electrolytes and Li metal triggers side reactions and decreases the CE by consuming the active Li metal. Desolvation of the solvent/anion molecules from the coordinating Li ion at the coating surface can solve this problem. Solid state electrolyte has ideally the highest selectivity for Li ion (transference number = 1), because Li ion migrates via hopping mechanism in the crystal structure. Abe and Janek et al. respectively reported that Li-ion transport at the interface between liquid electrolyte and solid state electrolyte has the highest activation energy and is the rate-limiting step [38,39]. This activation energy is related to the desolvation energy of solvent molecules from Li ion [38]. Additionally, Janek reported the formation of inorganic/organic composite layer at the interface between the solid state electrolyte and the liquid electrolyte, which increases the interfacial resistance [39].

Solid state electrolytes are the ideal coating material for selective transport of Li ions, however, the layer is brittle and usually has cracks and voids. At the plating step, Li metal can eventually grow through these defects and reach the liquid electrolyte. In contrast, polymer materials can realize uniform and defect-free coating thanks to the soft and

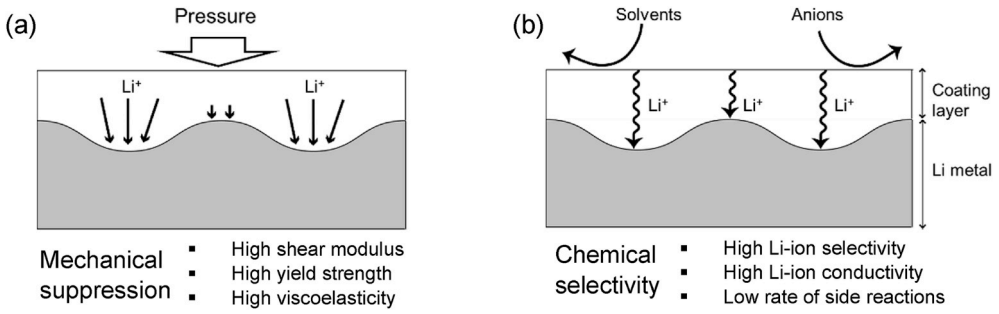

Fig. 2. (a) Mechanical suppression of dendrite growth. A coating layer with high shear modulus (>8 GPa) promotes Li metal deposition at the concave regions to reduce the surface roughness. (b) Selective conduction of Li cations through the coating layer. Less permeation of solvents and anions reduces the rate of side reactions with Li metal.

deformable nature. The disadvantage of using the polymer materials is, however, the selectivity toward Li ions is generally lower than the inorganic solid ion conductors. To enhance the selectivity of polymer coatings, understandings on the swelling ratio of polymer films in the electrolytes is critical, as this parameter is closely related to the chemical selectivity (or repelling ability) of the polymer against the solvents. For example, Whitesides et al. reported swelling ratio of PDMS in various solvent systems [40]. PDMS shows one order of higher swelling ratio in

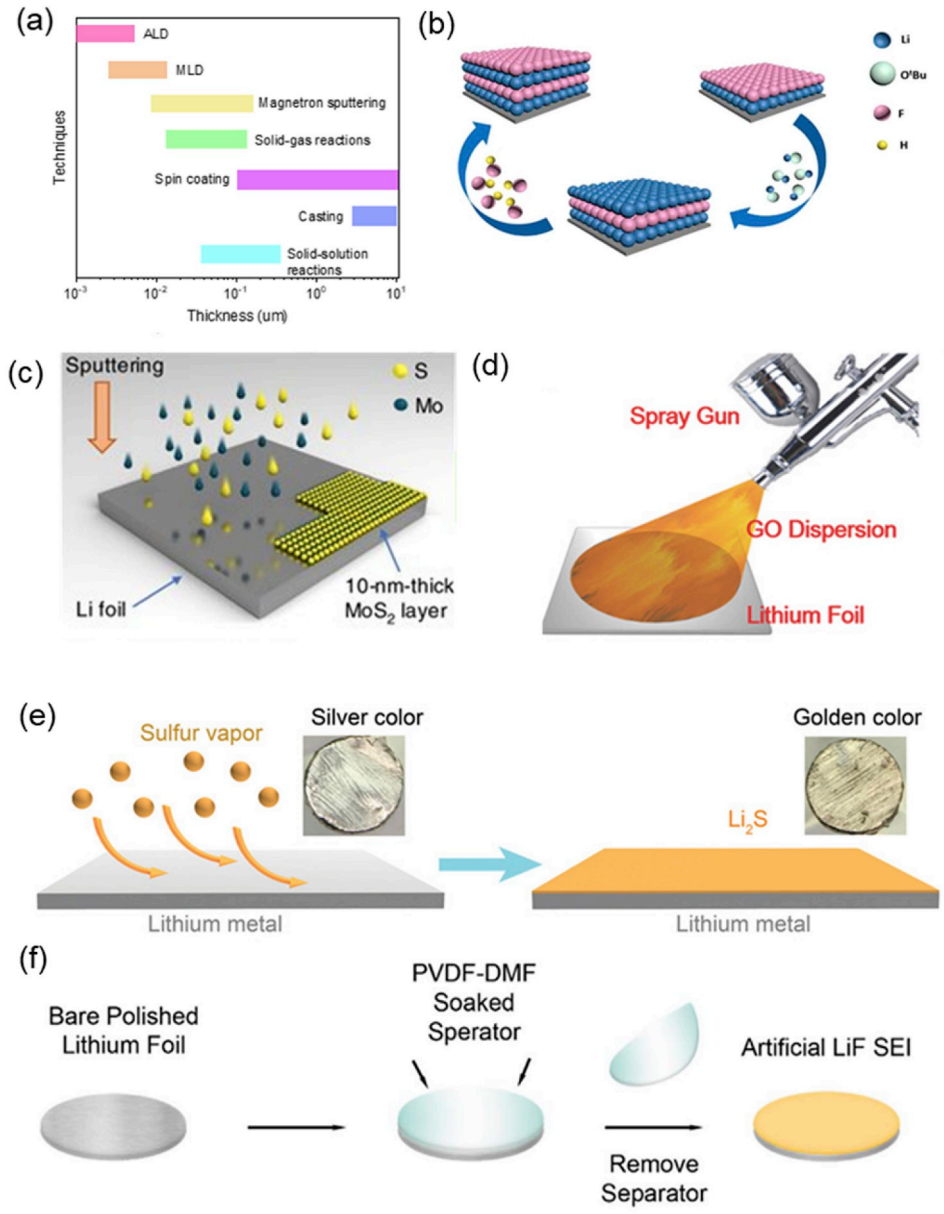

Fig. 3. (a) Thickness range of the protective coatings achievable by the various techniques. Versatile coating methods independent of surface reactivity of the substrate: (b) LiF coating on Li metal by ALD. Reproduced with permission. [42] Copyright 2018, American Chemical Society. (c) MoS_2 coating on Li electrodes by sputtering. Reproduced with permission. [48] Copyright 2018, Springer Nature. (d) Graphene oxide coating on Li foil by spray coating. Reproduced with permission. [57] Copyright 2018, John Wiley and Sons. Li-specific coating methods dependent on the reactivity of Li metal: (e) Li_2S coating produced from the reduction of sulfur vapor on Li metal surface. Reproduced with permission. [58] Copyright 2019, John Wiley and Sons. (f) LiF/polymer composite coating formed from the reduction of PVDF solution in DMF on Li metal surface. Reproduced with permission. [62] Copyright 2019, Elsevier.

ether solvent such as THF and dimethoxyethane than in carbonate solvent such as DMC. This result indicates PDMS film repels more carbonate solvent than ether solvent. It is important to note that less solvent in the polymer film results in lower ionic conductivity, because ion conduction is carried by the solvent molecules incorporated inside the polymer. Therefore, the balance between the chemical selectivity and ionic conductivity must be precisely tuned by swelling ratio of polymer film in the electrolyte.

To summarize, there are four major requirements for protective coatings in Li metal battery. 1) Uniform and crack-free coating layer to build a uniform current distribution over the entire electrode surface. High Li-ion flux at the cracks leads to dendritic growth of Li metal. On this point, flexible polymeric coatings have advantages over brittle inorganic coatings. 2) Mechanical properties such as high shear modulus, high yield strength, and high viscoelasticity of the coating help to suppress Li dendrite growth. High mechanical strength also enables the coating layer to survive long-term cycling of batteries. 3) Chemical selectivity toward Li ion over solvents/anions to reduce the rate of side reactions and increase the lifetime of Li metal anode. 4) High ionic conductivity, because a sluggish ion conduction builds up concentration gradient of Li ion and promotes dendritic plating of Li metal [19]. In addition, at high-rate charging/discharging, the energy loss by Ohmic resistance can be minimized by higher ionic conductivity.

3. Approaches for the formation of protective layers on Li metal surface

Various approaches have been reported to form protective coatings on Li metal surface. The range of obtainable thickness is dependent on the coating methods, as summarized in Fig. 3a. Depositions using gas-phase precursors (e.g. ALD, MLD, sputtering, see below) generally produce thinner coatings with thicknesses ranging from couple of nanometers to hundred nanometers. Methods using solution-phase precursors (e.g. spin, dip, cast, and spray coatings) generate submicron to a few micrometer thick coatings. Furthermore, the coating methods can be categorized into those using inert substrate (Fig. 3b–d), and those using reactivity of Li metal to initiate the formation of coating products (Fig. 3e and f).

ALD is a versatile technique of preparing high-quality thin layer of inorganic materials [41]. Based on the sequential and self-limiting chemical reactions, gaseous precursors deposit on a solid surface layer-by-layer at a growth rate of a few Angstroms per cycle [42]. For example, a thin film of LiF can be prepared by ALD from *t*-BuOLi and HF (Fig. 3b) [42]. In addition to the nanometer-level control of the thickness, ALD produces a smooth and uniform coating, which is beneficial for the protection of the electrode. MLD is a similar technique to ALD and can prepare organic or inorganic/organic hybrid films [43]. The organic components provide flexibility and functional groups to the film [44]. The working mechanism of MLD is pulsing two reactants to a solid surface alternatively and the polymerization takes place in a layer-by-layer manner. For instance, Sun et al. reported a fabrication of polyurea layer on Li metal by MLD from ethylenediamine and 1, 4-phenylene diisocyanate [45].

Sputtering is also a versatile coating technique and able to deposit nanometer-thick film of metal or oxide/sulfide materials on wide range of substrates [46–48]. Because sputtering technique only requires the vacuum environment and the external field to ionize the noble gas atoms, it is more cost-effective to produce inorganic thin films, compared to the ALD technique. MoS_2, (Fig. 3c), Al_2O_3, and Li_3PO_4 coating layer were successfully prepared on Li foil either by electron-based sputtering or by magnetron sputtering [47–49].

For a solution-based precursor, spin, dip, cast, and spray coating methods are used to form protective coatings. Spin coating produces a thin polymer film on a rotating disk as the liquid droplet is spread out by the centrifugal force while the solvent evaporates [50]. The coating thickness ranges from nanometers to a few micrometers and is controllable through the rotation speed and the concentration of the polymer solution. Dip coating is a simple method to produce a thin film by immersing the substrate into a polymer solution and drying in air. Multiple factors affect the thickness and morphology of the coating layer, such as surface condition of the substrate, the immersion time, the lifting speed, the number of dipping cycles, the operation temperature, and the humidity [51]. Cast coating is a scalable and versatile technique to make thin polymer films, often used in both laboratories and industries [52]. Thickness of coatings are tunable by various parameters, such as viscosity of the polymer solution, volatility of the solvent, and the drying temperatures. To prepare a film by cast coating, a homogeneous polymer solution is dropped on a flat substrate and casted with a blade, followed by a drying process. Cast coating is suitable for thin layer preparation in a range of sub-micrometers to micro-level thickness [53–55]. Spray coating uses a stream of fine droplets striking at the target substrates at high velocity to form a uniform layer [56]. This technique is suitable for mass production due to its high efficiency, low cost, and high reproducibility. For instance, Wei et al. employed spray coating technology to fabricate a graphene oxide layer on Li foil (Fig. 3d) [57].

Highly reactive surface of Li metal can be used as the initiator to grow protective coatings on top of the Li metal. The thickness of protecting layer can be controlled by the reaction time and the concentration of the reactant. Cui et al. used a solid-gas reaction of sulfur vapor on the reactive Li metal surface to form a homogenous Li_2S layer *in-situ* (Fig. 3e) [58]. LiF coating layers are prepared by the reduction of fluorine-containing gas on the Li metal surface [59,60]. Hybrid silicate is synthesized by reacting vapor of MPS and TEOS on the surface of Li metal [61].

Solid-solution reaction is also widely applied to produce a variety of coating materials on Li metal surface. Wu et al. reported a simple method to coat a uniform LiF/polymer composite layer on Li metal surface by reacting with PVDF dissolved in DMF (Fig. 3f) [62]. Polymerization of ethyl α-cyanoacrylate on the surface of Li metal was reported by Cui et al. [63] Li_3PS_4 layer is produced on Li metal surface inside the battery by the reduction reaction of Li_2S_6/P_2S_5 in an ether electrolyte [64].

4. Characterization techniques for physical and chemical properties of the protective coatings

The characterization of surface coating on Li mainly focuses on the composition, morphology, and mechanical property. Fig. 4 summarizes the tools for characterizing the coating layer, SEI layer, Li layer, and their interfaces. The EDX, XPS, XRD, FTIR, Raman spectroscopy, ED, and EELS are widely used for composition analysis. The morphology of the protective layer, SEI layer, and Li are studied by SEM and TEM. *In-situ* techniques for the analysis of electrode-electrolyte interfaces are reviewed in detail by Wang et al. [65].

XRD is a rapid analytical method used for crystalline phase identification. Benefiting from the high flux of synchrotron light sources, the current synchrotron-based XRD allows us to identify the nanometer-scale crystalline components such as Li, Li_2O, Li_2CO_3, and LiF in the SEI layer [58,66]. Furthermore, the *Operando* synchrotron XRD is currently under development, which is able to monitor the evolution of Li and crystalline SEI components throughout plating and stripping of Li. Consequently, this technique provides qualitative and quantitative information on chemically reacted Li, physically isolated Li, and electrochemically active Li in real time [1].

XPS is a surface-specific analytical tool probing the outermost region limited to 8–10 nm of the sampling depth. To avoid the reactions between Li sample and air, the XPS for Li metal study is usually equipped with an argon filled glovebox. Another approach to eliminate the air contamination is using a custom-designed, air-tight sample holder to transfer the sample from glovebox to the XPS instrument. In addition to identify the chemical species, XPS can quantify the ratio of chemical

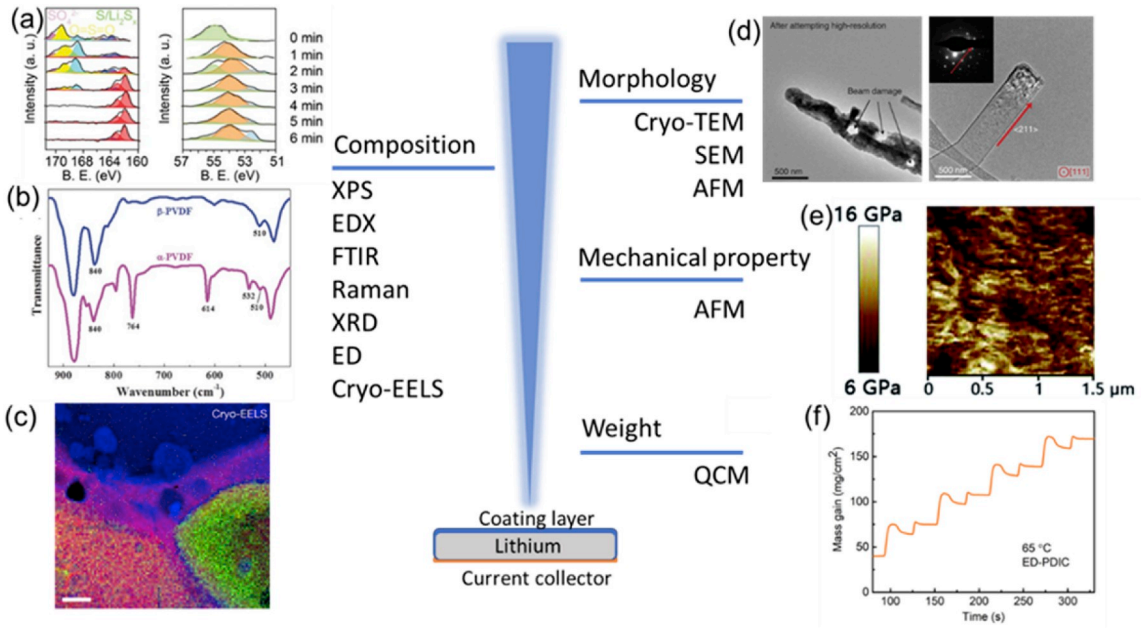

Fig. 4. Characterization techniques for the coating layers or the SEI layers on lithium metal anode: (a) Depth profile of the XPS spectra of Li_2-S coating layer on Li metal after varied sputtering times. Reproduced with permission. [58] Copyright 2019, John Wiley and Sons. (b) FTIR spectra of α-phase and β-phase PVDF coatings. Reproduced with permission. [67] Copyright 2017, John Wiley and Sons. (c) EELS elemental mapping of the SEI layer on Li metal. Reproduced with permission. [73] Copyright 2018, Springer Nature. (d) TEM images of the Li metal dendrite observed under standard TEM (left); and under cryo-TEM (right), which is free from the beam damage. Reproduced with permission. [71] Copyright 2017, The American Association for the Advancement of Science. (e) AFM image of Li_3P/LiCl composite layer showing high Young's modulus of the coating. Reproduced with permission. [75] Copyright 2018, Royal Society of Chemistry. and (f) QCM analysis of the mass gain of polyurea thin film growing on Li metal. Reproduced with permission. [45] Copyright 2018, John Wiley and Sons.

compounds at the sample surface. By etching the surface layer, the depth profile of the chemical compositions from the outermost surface layer to the bulk regions can be analyzed [22,58]. The depth profile of the coating layer produced from the solid-gas reaction of sulfur vapor and Li metal are shown in Fig. 4a as an example [58]. According to the S 2p and Li 1s spectra, the outmost layer of the coating is composed of multiple compounds such as Li_2CO_3, Li_2S, $LiSO_3$, $LiSO_2$, and Li_2SO_4. In contrast, the main components from the middle to the bulk layer are simply Li_2S and Li_2CO_3. The gradation of sulfide compounds represents that the degree of sulfur reduction varies with the distance from the reductive surface of Li metal.

FTIR and Raman spectroscopy are often employed to analyze the composition of Li metal surface [55,61,62,67]. ATR-FTIR is particularly sensitive to the sample surface and suitable for the surface analysis. For example, a thin PVDF film coated on Cu current collector is analyzed by this technique (Fig. 4b) [67]. ATR technique can be applied to *in-situ* analysis of SEI composition on the anode surface [68]. As such, *in-situ* characterization of the protective coating during plating/stripping of Li metal can potentially provide useful information on the swelling behavior or the compositional change in the coating. *In-situ* stimulated Raman scattering has been demonstrated to monitor the concentration gradient of anion at the electrolyte-Li interface, and the growth of Li metal under a Li_3PO_4 coating [19].

SEM is frequently used to study the morphologies of the coating layer, the cross-sectional interface layer. Observation of Li metal electrodeposited after varied times provides the time evolution of nucleation and growth of Li metal particles or the dendrites inside the battery cell [34,69]. The intensity of electron beam used in SEM is much lower than TEM, and therefore minimum beam damage is expected in SEM [70]. However, the resolution of SEM is not high enough to observe a nanometer-thick coatings (those formed by ALD or sputtering techniques) and the SEI layer. In contrast, TEM enables observation of SEI layer under the high-energy electron beam. The challenge of TEM characterization has been the beam damage to thin Li and organic samples (Fig. 4d, left), and then cryo-TEM which operates at cryogenic temperature is developed by Cui [71], Meng [72], Kourkoutis et al. [73], respectively, to minimize the beam damage on Li metal (Fig. 4d, right) [71].

A few other analytical tools for elemental or chemical characterizations are often paired with electron microscopies. EDX is generally combined with SEM to provide elemental mapping along with sample morphology. Elemental Li is inactive in EDX analysis and therefore observed as a black region in the EDX mapping image. The cross-sectional EDX mapping of the coated Li metal is able to identify the thickness and uniformity of the coating layer on the Li metal. For example, cross-section of the MoS_2-coated Li metal was characterized by Mo and S signals in the EDX analysis, which shows that MoS_2 layer on Li foil is structurally stable, and the uniform film is observable after 300 cycles. [48].

EELS provides abundant chemical information of the sample such as the atomic composition, chemical bonding, and valence number. EELS instrument is generally combined with TEM. In contrast to EDX, signals from light elements such as Li is observable in EELS. Electron diffraction is another analytical technique combined with TEM imaging to determine the crystal structure of the sample at a particle or even at an atomic level. Because high-energy electron beam can damage organic samples and Li metal, cryogenic condition has been used in EELS (Fig. 4c) [73], and electron diffraction (Fig. 4d, inset) [71], to evaluate the chemical composition or determine the crystal orientation of Li metal and the SEI layer [74]. Kourkoutis et al. combined cryo-STEM and EELS to obtain the nanoscale structure and composition of intact SEI on Li metal, revealing the structure of Li dendrites and the SEI layers [73].

AFM probes the surface morphology and mechanical properties of the samples, which achieves high vertical resolution of 0.1 nm [63]. AFM is unique for its capability of evaluating the Young's modulus of the coating layer by measuring the van der Waals forces between the

probing tip and the surface [22,75]. Qian measured the mechanical properties of Li_3P/LiCl coating layer on Li metal by AFM in peak force tapping (PFT) mode. As shown in Fig. 4e, Li_3P/LiCl layer on the Li surface shows high Young's modulus, which suppresses the growth of Li dendrites [22,75].

QCM techniques measure nanogram-scale mass changes of the electrode during the electrochemical reactions [76,77]. For instance, Sun et al. used QCM to evaluate the growth rate of polyurea on Li foil (Fig. 4f) [45]. QCM can quantify and accurately control the film thickness coated on Li foil, which has prominent influence on the ionic conductivity of the film.

5. Morphology of Li metal and electrochemical method to evaluate the protective function of coating layers

Protective effects of a coating layer on Li metal are usually evaluated by observation of the morphology of electroplated Li metal, electrochemical performance in a Li||Li symmetric cell, Cu||Li cell, and Li|| cathode full cell. An effective coating layer leads to a dense and dendrite-free deposition of Li metal even after extensive numbers of cycles. Long cycle life and stable voltage curve in Li||Li symmetric cell, especially under large current and capacity, indicate stable deposition of Li metal. CE in plating/stripping cycle of Li metal can be evaluated by Cu||Li cell and enables a quantitative evaluation of Li loss during the cycles. Practical application of a protective coating can be assessed by cycling the protected Li metal anode paired with a cathode. We briefly summarize the key information obtainable from these characterization and cell testing, the required condition for the testing, and the way of interpreting the results. This section is intended to make the comparisons of the protection performance more comprehensive between different coating materials as discussed in Section 6 and 7.

5.1. Morphology of Li metal

SEM is a common tool to study the morphologies of the coating layer and deposited Li. SEM analysis provides three key information. 1) Position of electrodeposited Li metal. To exert the protective function of the coating layer, Li metal has to be deposited underneath the coating layer. 2) Morphology of electrodeposited Li metal particles. Round shape and large particles (>5 μm of diameter) has smaller contact area with the electrolyte than fibrous and dendritic shape, and thus less side reaction is expected [8]. 3) Total thickness of deposited Li metal on the current collector. To reduce the contact area with the electrolyte, low pore volume inside the deposited Li metal is desirable. The porosity in Li metal can be evaluated from the total thickness of deposited Li metal. A useful standard is that 1 mAh cm^{-2} of Li metal with zero porosity yields a deposition thickness of 4.85 μm. Assuming an isotropic pore, total thickness as d μm, the porosity in Li metal deposited after Q_p mAh cm^{-2} can be calculated from the formula, $(d - 4.85Q_p)/d$.

5.2. Li||Li symmetric cell cycling

Cycling the Li||Li symmetric cell at different current densities with various areal capacities is the first approach to assess the performance of the surface protected Li. Voltage curves reflect the morphology evolution of Li metal. There are two typical symptoms of cell failure due to the Li dendrite growth (Fig. 5a). The voltage suddenly drops to 0 V as a result of Li dendrites penetrating the separator and shorting the cell (Fig. 5b, pure Li metal) [58]. Another phenomenon is the dramatic increase of the cell polarization, which is also associated with dendritic Li formation leading to high surface area porous Li deposition (Fig. 5b, Li_2S_8 preplant Li). The Li metal with high surface area not only reacts with the electrolyte to generate highly resistive side reaction products,

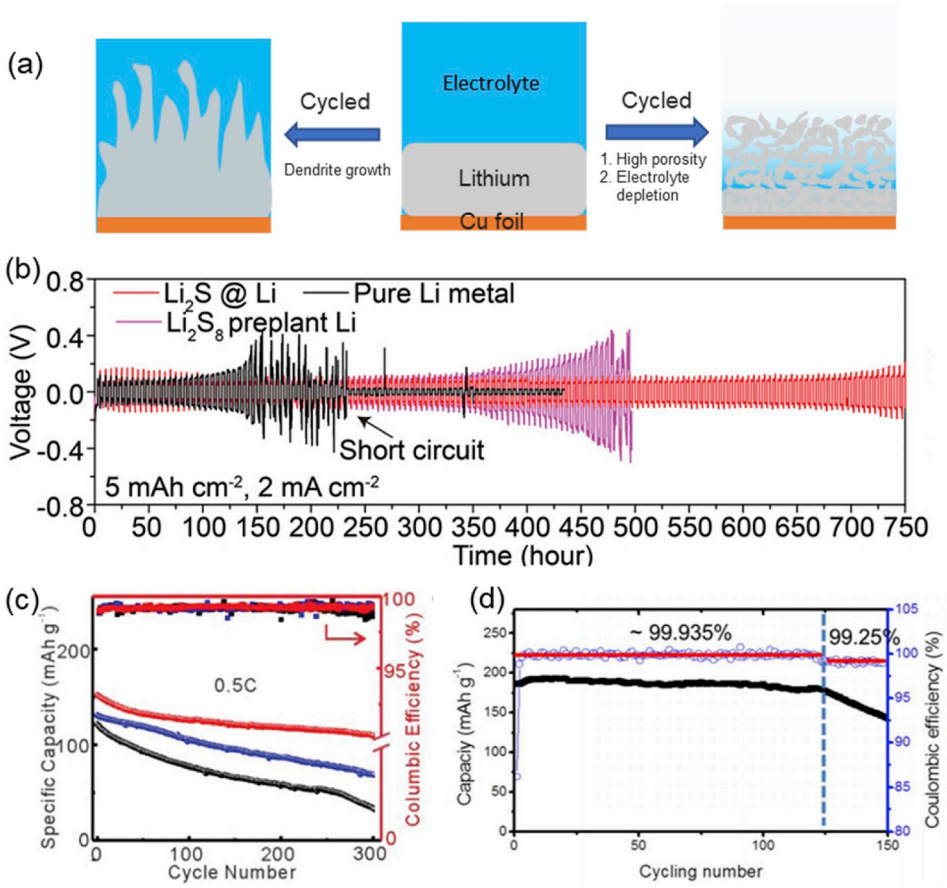

Fig. 5. (a) Schematic diagram of two possible Li failure mechanisms. (b) Li||Li symmetric cell cycling with/without coating. Reproduced with permission. [58] Copyright 2019, John Wiley and Sons. (c) Cycling stability of Li||LCO cells tested under 17-fold excess amount of Li metal. Reproduced with permission. [79] Copyright 2019, John Wiley and Sons. (d) Cycling stability of Li||NMC811 cells tested with one-fold excess of Li metal. Reproduced with permission. [80] Copyright 2018, Springer Nature.

but also absorbs the electrolyte into the pores. Although the cell is not shorted, the increase of the polarization and unstable voltage curves indicate massive Li dendrites formation. Long-term cycling without apparent increase of voltage polarization is a good indication of stabilization of Li metal (Fig. 5b, Li_2S-coated Li). Because Li metal becomes less stable at higher current density and higher capacity, Li||Li cycling test at such conditions can clearly show the validity of protective coatings. It is worth mentioning that the Li||Li cycling test fails to distinguish the internally-shorted cell, when the voltage curve appears smooth and stable for long period of time, while the voltage does not reach 0 V (often referred as soft short). Then, EIS test is required to prove the cell is not shorted.

5.3. Coulombic efficiency

CE test is conducted in a two-electrode cell with Cu as the working, and Li as both counter and reference electrodes. Li metal is repetitively plated on and stripped from Cu electrode. CE is calculated from the ratio of stripping capacity to plating capacity ($CE = Q_s/Q_p$). CE less than unity means loss of Li metal in the plating/stripping cycles. Influence of current density, Q_s, and Q_p on CE and other cycling protocols is detailed elsewhere [78]. The irreversible loss of the Li originates from either chemical reaction with the electrolyte to form SEI, or formation of electrically isolated Li particles. The effectiveness of a protective coating is evaluated by comparing the CEs with or without the coating covered on the Cu working electrode. An effective coating layer suppresses the irreversible chemical reaction by reducing the contact between the Li and electrolyte, and mitigates the formation of isolated Li metal particles by promoting dense uniform Li deposition.

5.4. Full cell

Li||cathode full cell is the ultimate evaluation of the coating, which provides insight for practical application. Depending on the compatibility between the coating and the electrolyte solvent, the cathode for the full cell testing is usually LFP, sulfur, and NMC. Although there are reports of stable cycling at high current densities in Li||Li cells, the reported current density used in Li||cathode full cell is usually much lower than the value used in Li||Li cells. Cathode with high loading of active materials are required to test the full cell at higher current density. The benefits from the coating are obvious when limited Li and/or lean electrolyte is used. For instance (Fig. 5c), high CEs of >99.8% are reported as Li efficiencies with more than 10-fold excess of Li in the full cell. However, the excess Li means the reported efficiency value is really a measure of the cathode reversibility [79]. In comparison, Fig. 5d shows the performance of Li||NMC 811 cells with one-fold excess of Li. Before the excess Li is consumed the capacity of the cell is stable and the CE is 99.93%, which represents the CE of the cathode [80]. Once the excess Li is consumed, the capacity of the cell decay much faster and the CE of the cell reflects the efficiency of the Li anode. Since the CE of the full cell with excess Li is basically the CE of the cathode, a proper way to evaluate the CE of Li metal in a full cell is to test the anode free cell, which only utilize the Li from cathode side.

6. Inorganic coating

Inorganic coatings generally possess high shear modulus and can serve as a physical barrier to Li metal dendrite [26,28]. Table 1 lists the intrinsic shear modulus and ionic conductivity of inorganic materials used as the protective coating on Li metal. Al_2O_3, fluorinated graphene (GF), LiF shows notably high shear modulus, while sulfide-based materials such as MoS_2 and Li_3PS_4 shows lower shear modulus. Materials with high ionic conductivity is expected to transport Li cations via hopping mechanism and show the highest selectivity toward Li cations. Meanwhile, ion transport through non-conductive coating layer is only possible in the liquid electrolyte permeating the layer, and therefore, the selectivity toward Li ion through non-conductive layer is limited. In short, high ionic conductivity of inorganic coating materials directly leads to high selectivity of Li cation. This relation is only true for single-ion conductor and not true for polymeric materials (Section 7).

Coating uniformity is the essential factor which determines the performance of inorganic coating. Presence of defects, grain boundaries, and pores in coating layer significantly reduce shear modulus, ionic conductivity, and the Li^+ selectivity. Most of the inorganic coatings is directly formed on the Li surface by ALD, sputtering, or solution-phase reaction (Table 1). Then, high-pressure compression or high-temperature sintering to eliminate the defects in the coating layer is not available [81], because those processes result in deformation or melt-down of metallic Li.

Performance of inorganic coating is often evaluated as the cycling

Table 1
Conditions and cycle numbers of Li||Li symmetric cells with various inorganic coatings on the Li metal. Note thick Li metal foil (>250 μm) is used in the test. Reference for ionic conductivity at room temperature: LiF = ref [82]; Al_2O_3 = ref [83]; LiPON($Li_{3.3}PO_{3.8}N_{0.22}$) = ref [84]; Li_3PS_4 = ref [81]; Li_3P = ref [85], Reference for shear modulus: LiF/LiCl = ref [86]; Al_2O_3 = ref [87]; LiPON = ref [88]; Li_3PS_4 = ref [89]; MoS_2 = ref [90]; GF = ref [91].

Material	Ionic conductivity (S cm^{-1})	Shear modulus (GPa)	Coating method	Thickness	Electrolyte	Current (mA cm^{-2})	Capacity (mAh cm^{-2})	Cycle number	Ref.
LiF	10^{-13}-10^{-7}	76 (LiF)	ALD	8 nm	EC/EMC (3:7), 1 M $LiPF_6$	1	1	130	[42]
LiF	10^{-13}-10^{-7}	76 (LiF)	Solid-gas reaction	380 nm	EC/DEC (1:1), 1 M $LiPF_6$	5	1	300	[60]
LiF + polymer	10^{-13}-10^{-7}	76 (LiF)	Solution reaction	300 nm	EC/DEC (1:1), 1 M $LiPF_6$	3	1	300	[62]
Al_2O_3	10^{-30} (amorphous Al_2O_3)	165 (Al_2O_3)	Magnetron sputtering	20 nm	EC/DEC/DMC (1:1:1), 1 M $LiPF_6$	0.5	0.5	600	[47]
LiPON + polymer	2.4×10^{-6} (LiPON)	31 (LiPON)	ALD	15 nm	EC/DEC (1:1), 1.5 M $LiPF_6$	2	2	100	[92]
Li_3PS_4 +LSPS	3×10^{-4} (Li_3PS_4)	8.7 (Li_3PS_4)	Solution reaction	2 μm	DOL/DME, 1 M LiTFSI, 25 mM Li_2S_6/P_2S_5	4	1	800	[64]
Li_3P + LiCl	10^{-4} (Li_3P)	34 (LiCl)	Solution reaction	15 μm	EC/DMC/EMC (1:1:1), 1 M $LiPF_6$, 5% FEC	3	2	100	[75]
$Li_{13}In_3$ + LiCl	Mixed conductor	–	Solution reaction	10 μm	DOL/DME (1:1) 1 M LiTFSI	2	2	600	[93]
MoS_2	Mixed conductor	18 (MoS_2)	Sputtering	10 nm	DOL/DME (1:1), 1 M LiTFSI, 0.25 M $LiNO_3$	10	5	300	[48]
GF + LiF	Mixed conductor	140 (GF)	Solid-solid reaction	1 μm	EC/DEC (1:1), 1 M $LiPF_6$	10	1	165	[94]

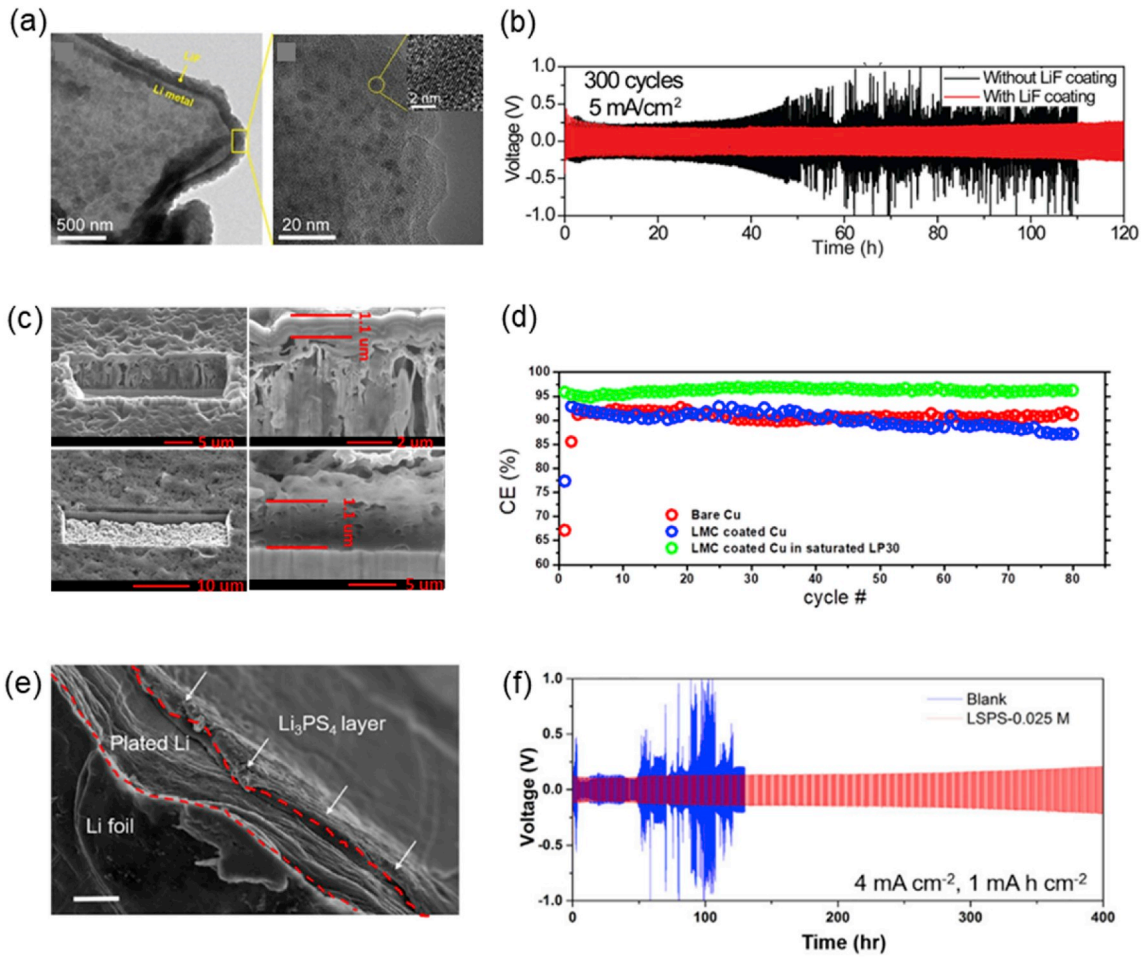

Fig. 6. (a) TEM images of LiF coating on Li metal surface. (b) Li||Li symmetric cell cycling in EC/DEC electrolyte at 5 mA cm^{-2} and 1 mAh cm^{-2} with/without LiF coating. Reproduced with permission. [60] Copyright 2017, American Chemical Society. (c) Cross-sectional SEM images of Cu current collector after 1 mAh cm^{-2} of Li metal is deposited (top) and then stripped (bottom) in 0.2 M LiI EC/DMC solution. A layer of 1 μm-thick lithium methyl carbonate (LMC) is observed on the surface. (d) CE of Li plating/stripping on Cu current collector without coating, with LMC coating in normal LP 30 electrolyte (EC/DMC + 1 M $LiPF_6$), and with LMC coating in LP30 electrolyte saturated with LMC. Reproduced with permission. [108] Copyright 2018, American Chemical Society. (e) Cross-sectional SEM image of Li metal after 4 mAh cm^{-2} of Li is plated in 0.025 M of L_2S_6/P_2S_5 (LSPS) ether solution. A layer of Li_3PS_4 is formed on the Li surface. Scale bar = 20 μm. (f) Li||Li symmetric cell cycling at 4 mA cm^{-2} and 1 mAh cm^{-2} in DOL/DME electrolyte added with L_2S_6/P_2S_5. Reproduced with permission. [64] Copyright 2017, Elsevier.

life of Li||Li symmetric cell (Table 1). Longer cycle numbers at higher current density and higher capacity indicate superior protection effect on the Li metal. However, one must note that Li metal foil used in the cell is usually very thick (>250 μm), corresponding to nearly 50 mAh cm^{-2} in capacity. Given such an excess amount of Li as a reservoir, the cycle life of the cell is determined by the rate of electrolyte consumption or cycle life before internal shorting, rather than by the consumption rate of metallic Li. Measurement of CE or use of thin (controlled amount of) Li foil is highly recommended to evaluate the reduction rate of side reactions by protective coatings (Section 5.3).

6.1. Ionically non-conductive materials

6.1.1. Lithium halide

LiF is a major SEI compound formed from the decomposition of fluorinated salts or fluorinated organic solvents [95–97]. Because Li metal generally shows stable cycling in those fluorinated electrolytes, LiF is believed to protect Li metal surface. Rochefort et al. reported that Li metal immersed in FEC solvent can be cycled in acetonitrile (1 M $LiPF_6$ as the salt), a solvent known to react with Li metal [98]. XPS and AFM analysis of the SEI layer on Li metal after the immersion in FEC revealed the presence of LiF, Li_2CO_3, and polymeric compounds. The authors suggested that the soft polymeric components also play the important role in protecting Li metal surface.

Mechanism of ion transport and the exact ionic conductivity in LiF is still unclear today. A theoretical study showed defects in LiF can contribute to the ionic conductivity [99]. Pan et al. shows Schottky pairs are likely formed at the anode side, and the ionic conductivity of LiF is estimated as 10^{-31} S cm^{-1}. On the cathode side, *p*-type defect is formed, and the ionic conductivity of LiF is estimated as 10^{-12} S cm^{-1}. The authors suggested doping divalent cation (e.g. Mg^{2+}) in LiF increases the carrier concentration and improve the ionic conductivity. Greeley et al. calculated the conductivity of LiF to be in the range of 10^{-7}-10^{-13} S cm^{-1}, much higher than the value reported by Pan et al. [82] Li et al. reported that LiF thin film deposited on silica (0001) surface is structurally disordered, and the ionic conductivity is experimentally evaluated as 6×10^{-6} S cm^{-1} at 50 °C [100]. The cause of high conductivity is attributed to the interface region between the amorphous and the crystalline phases in LiF. The authors reported thermal annealing of the LiF film at a moderate temperature (350 °C) is the key to growing the amorphous-crystalline interface.

Several methods have been reported to form LiF layers directly on Li metal. Elam et al. used ALD with *t*-BuOLi and HF as the precursors [42]. Cui et al. produced LiF layer by the direct reaction of fluorine (F_2) gas on Li metal surface (Fig. 6a) [60]. The F_2 gas is generated from thermal decomposition of perfluoro-3-butenyl vinyl ether (commercially known

as Cytop) and diffuses to the Li surface to initiate the formation of LiF. Li||Li symmetric cell with the LiF layer (380 nm) cycles for 300 cycles at 5 mA cm^{-2}, 1 mAh cm^{-2} in an electrolyte composed of EC and DEC with 1 M of $LiPF_6$ (Fig. 6b). Wu et al. reported that Li metal immediately reacts with a DMF solution of PVDF to form a composite film (300 nm thick in total) of LiF and polymers derived from PVDF [62]. Li||Li symmetric cell with the LiF/polymer coating cycles for 300 cycles at 3 mA cm^{-2} and 1 mAh cm^{-2} in a carbonate electrolyte (EC/DEC (1:1) + 1 M $LiPF_6$).

LiCl is another Li halide salt having higher shear modulus (34 MPa) than Li metal. Yang et al. prepared a LiCl/polymer composite layer from the reaction between C_2Cl_4 and LiOH on the Li metal surface [101]. Lithiophilic nature of LiCl surface facilitates the Li^+ transport through the composite layer. The surface-modified Li||Li cell cycles for 1000 h without increase of voltage hysteresis at 2 mA cm^{-2} and 1 mAh cm^{-2} in ether electrolyte (DOL/DME + 1 M LiTFSI + 2% $LiNO_3$).

6.1.2. Aluminum oxide

An ultrathin coating of Al_2O_3 is commonly prepared by ALD technique (Section 3), using a reactive organometallic precursor (trimethylaluminum) and water vapor. Nanometer-thin amorphous Al_2O_3 layer has been proven to protect cathode materials from the decomposition reaction by HF in the electrolyte [102]. To understand the ion transport through amorphous Al_2O_3 layer, Wolverton et al. calculated the Li diffusivity as 2.7×10^{-14} m^2 s^{-1} at 600 K [83]. Based on this result, the conductivity of Al_2O_3 is estimated as only 10^{-30} S cm^{-1} at 300 K. Such low ionic conductivity requires Al_2O_3 layer to be nanometer-thin to allow Li^+ diffuse through.

On the surface of Li metal, reduction of Al_2O_3 produces $LiAl_5O_8$ phase. Recent ab initio calculation shows $LiAl_5O_8$ has a lower Li-ion migration barrier (0.33 eV) and higher Li-ion diffusivity (3.6×10^{-8} cm^2 s^{-1}) than Al_2O_3 (2.69 eV, and 9.3×10^{-48} cm^2 s^{-1}, respectively) [103]. Therefore, $LiAl_5O_8$ coating layer is expected to be a more ideal single-ion conductive coating layer than Al_2O_3.

Hu et al. coated ultrathin layer of Al_2O_3 on a garnet Li-ion conductor, LLCZN [104]. The lithiophilic nature of Al_2O_3 interface layer results in intimate contact between the Li metal and LLCZN, and the interfacial impedance is reduced significantly. TEM/EELS analysis reveals that Al_2O_3 is converted into $Li_2Al_4O_7$ (another Li-ion conductive phase) at the interface with Li metal. Their study provides a perspective for solving the inherent problem of high interfacial resistance in all-solid-state Li metal batteries [105].

Li et al. used magnetron sputtering to coat Al_2O_3 layer directly on Li surface [47]. The authors compared the Li||Li cycling life with different thickness of Al_2O_3 layer (0, 7, 20, 40 nm) in a carbonate electrolyte, and 20 nm-thick Al_2O_3 layer showed the longest cycling life (>1000 h at 0.5 mA cm^{-2}, 0.5 mAh cm^{-2}). Interestingly, the authors observed Li metal deposited on top of the Al_2O_3 layer rather than underneath the layer. This result indicates the ionic conductivity of 20-nm-thick Al_2O_3 layer is too low, and Li metal deposits through the cracks in the Al_2O_3 layer.

6.1.3. Lithium methyl carbonate

LMC is another class of SEI component often observed in carbonate electrolytes [106]. Liu et al. demonstrated that a uniform coating of LMC can be formed on Li metal surface by a selective demethylation of DMC, catalyzed by LiI (Fig. 6c) [107–109]. Because LMC is soluble in EC/DMC solvent, the electrolyte is saturated with LMC powder to suppress the dissolution of the LMC coating layer. The CE of Li deposition of LMC-coated Li metal in LMC-saturated carbonate electrolyte (EC/DMC (1:1) + 1 M $LiPF_6$ + sat. LMC) is 96%, which is higher than the efficiency in a commercial LP30 carbonate electrolyte (EC/DMC (1:1) + 1 M $LiPF_6$) (Fig. 6d) [108].

6.1.4. Lithium sulfide

Li_2S is often observed on the Li metal anode in Li||S batteries due to the reaction between polysulfide and Li metal [110]. Although the formation of Li_2S on the anode decreases the amount of active sulfur, the solid Li_2S layer is believed to hinder the growth of Li dendrite. Cui et al. made a dense layer of Li_2S (62 nm thick) on Li surface via solid-gas reaction between vaporized sulfur and solid Li metal [58]. The CE of Li deposition is evaluated by measuring the consumption rate of thin Li metal anode (10 mAh cm^{-2} capacity) in a ether electrolyte (DOL/DME (1:1) + 1 M LiTFSI), and the efficiency is 98.9%.

6.2. Ion-conductive materials

6.2.1. Lithium phosphorous oxynitride

LiPON is an amorphous solid-state electrolyte, which can be prepared either by radio frequency reactive sputtering or ALD techniques. Xie et al. coated 2 μm-thick LiPON on both Cu current collector and Li metal, each of which were assembled into a pouch cell [111]. The authors demonstrated prolonged cycle life in both LiPON-coated Cu||$LiCoO_2$ cell and LiPON-coated Li||$LiCoO_2$ cell. However, when NCA and elemental sulfur are used as the cathode materials, LiPON coating deteriorates the cycle life. Because the capacity of NCA and sulfur is higher than the $LiCoO_2$, larger amount of Li metal is deposited during the charging cycle, which leads to the crack formation in LiPON layer and eventually causes the deterioration of the cycling performance.

To overcome this brittle nature of LiPON, Noked et al. put a 800-nm-thick polymer layer underneath a LiPON layer (15 nm) [92]. The polymer layer is prepared by electrochemical polymerization of DOL on Li metal surface. However, thermal expansion of the underlying polymer layer during the 150 °C ALD process results in formation of cracks in the top LiPON layer. After 100 cycles of plating/stripping, electroplated Li metal is observed at the surface cracks in LiPON layer. Although the surface of Li metal is exposed to the electrolyte, the morphology of Li metal was smooth and densely packed on top of the LiPON layer. This result indicates that the surface composition of the substrate can alter the electroplating behavior of Li metal.

6.2.2. Lithium phosphorous sulfide

Li_3PS_4 is a glassy solid-state electrolyte widely used in solid state Li metal battery. Compared to garnet type solid electrolyte, Li_3PS_4 is more malleable and ductile, offering great processing ability to form a thin film [112]. Li_3PS_4 can be synthesized from a solution phase, which enables a facile way to form a uniform coating on Li metal surface [113]. Nazar et al. formed Li_3PS_4 coating directly on Li surface by soaking a Li foil into a DOL/DME mixed solution of Li_2S_6 and P_2S_5 [64]. The resulting layer is a mixture of conductive Li_3PS_4 and non-conductive phosphorous sulfide species. Thickness of the resulting Li_3PS_4 coating was approximately 2 μm (Fig. 6e). In the electrochemical test, Li_2S_6 and P_2S_5 are added directly into the electrolyte to form Li_3PS_4 layer *in-situ* on the surface of Li metal electrode. As a result, Li metal can be stably plated/stripped for 400 h at a high current density of 4 mA cm^{-2} (Fig. 6f), and no dendritic nor mossy Li is observed during the cycling under the optical microscopy. Sun et al. used an alternative pathway to form Li_3PS_4 layer on Li metal surface, where Li foil is soaked in a solution of P_4S_{16} in NMP [114]. The authors showed improved capacity retention of Li||S battery with the Li_3PS_4 coating.

6.2.3. Lithium phosphide

Yang et al. prepared Li_3P from the direct reaction between Li metal and PCl_3 [75]. Li_3P is known as a fast Li-ion conductor (10^{-4} S cm^{-1} at room temperature) [85]. The overpotential of Li_3P-coated Li||Li symmetric cycling is reduced and achieves 100 cycles at 3 mA cm^{-2} and 2 mAh cm^{-2} in a carbonate electrolyte (EC/DMC/EMC (1:1:1) + 1 M $LiPF_6$ + 5% FEC).

6.3. Mixed ion-electron conductor

6.3.1. Composite of metal and lithium halide

Nazar et al. formed a layer of lithium alloy (e.g. $Li_{13}In_3$, LiZn, Li_3Bi,

Li_3As) by soaking a lithium metal in THF solution of metal chloride (MCl_x; M = In, Zn, Bi or As) [93]. LiCl is a byproduct in the reaction and remained in the alloy layer. The $Li_{13}In_3$ coating layer shows particularly effective protection on Li metal. $Li_{13}In_3$-coated Li||Li symmetric cell cycles for 1200 h at 2 mA cm^{-2} and 2 mAh cm^{-2} in an ether electrolyte (DOL/DME (1:1) + 1 M LiTFSI).

Xie et al. prepared a composite Li–Sn alloy/polymer layer by soaking a Li metal into a THF solution of $SnCl_4$ [115]. $SnCl_4$ reacts with Li metal to form Li–Sn alloy and LiCl, while THF polymerizes into PTMEG. Li metal with the composite coating becomes more resistant against water. With the Li–Sn/polymer coating, Li||Li cycling achieves 1000 h at 1 mA cm^{-2}/1 mAh cm^{-2} in an ether electrolyte (DOL/DME + 1 M LiTFSI + 1 wt% $LiNO_3$). In addition, a Cu||Li cell achieves 200 cycles at 0.5 mA cm^{-2}/1 mAh cm^{-2} with a CE of over 95%.

Yan et al. reported a LiF/Cu composite layer prepared by the reduction of CuF_2 on the Li metal surface [116]. LiF/Cu layer is a mixed conductor, and the electronic and ionic conductivities are 2.06×10^{-3} S cm^{-1} and 1.79×10^{-4} S cm^{-1}, respectively. CE of Li metal covered with LiF/Cu layer is evaluated as 96.3% under 0.5 mA cm^{-2} with 0.5 mAh cm^{-2} in a carbonate electrolyte (EC/DEC (1:1) + 1 M $LiPF_6$).

6.3.2. 2D materials and carbon nanotube

2D materials such as graphene, GO, GF, and MoS_2 can conduct Li ion in between the layered structures. These layers are highly selective toward Li ion and expected to expel the solvent molecules from the Li metal surface. Cui et al. studied electroplating of Li metal on Cu foil where the surface is covered with boron nitride or graphene nanosheets [117]. Li metal plating through the 2D layers forms dense morphology, and the CE is increased to 97% at the cycling condition of 0.5 mA cm^{-2} and 5 mAh cm^{-2} in a carbonate electrolyte (EC/DEC + 1 M $LiPF_6$). Choi et al. coated MoS_2 layer directly on Li metal via sputtering technique (Section 3) [48]. The authors demonstrated stable cycling of MoS_2-coated Li metal at high current density (10 mA cm^{-2}) and large capacity (5 mAh cm^{-2}).

Qian et al. reported a composite coating of LiF with graphene fluoride (GF), which was prepared by reacting GF with molten Li metal [94]. The GF-LiF coating suppresses growth of Li dendrite and enables stable Li||Li cycling at high current density (10 mA cm^{-2}) in a carbonate electrolyte. The coating is hydrophobic and protects Li metal from moisture damage when exposed to ambient air.

Carbon nanotube (CNT) is an electron conductive material, and Li metal is expected to grow on the top when placed on Li metal anode. However, lithiophobic nature of CNT prohibit Li metal to deposit directly on CNT surface. Zhang et al. prepared a multilayer ZnO/CNT coating film with lithiophilic-lithiophobic gradient where the inner layer of CNT is coated with ZnO to alter the surface nature to be more lithiophilic, while the outer layer of CNT remains bare and lithiophobic [118]. The gradual increase of lithiophilicity of the ZnO/CNT film towards Li metal surface guides uniform deposition of Li metal underneath the coating layer. Stable Li||Li cycling was demonstrated under 10 mA cm^{-2} with 1 mAh cm^{-2} in coin cell, and 1 mA cm^{-2} with 1 mAh cm^{-2} in pouch cell.

7. Polymer and polymer/inorganic composite coatings

Polymer coatings are more flexible and elastic compared to inorganic coatings and thus more capable of accommodating volume change during Li plating/stripping. Intimate contact between polymer layer and Li metal is often observed, because polymer itself or the liquid that swells the polymer wets the surface of Li metal better than rigid inorganic precursors. Polymer can be made into a uniform film by spin coating, solution casting, and even direct polymerization on Li metal surface. Thickness is controllable by the concentration of the polymer solution used in the coating process or by the reaction times. Thinner coating can increase the ionic conductivity of the polymer film, while thicker coating can enhance the film toughness and the selectivity toward the conduction of Li^+ [119].

In addition to film thickness, ionic conductivity of polymer films depends on the swelling ratio in the electrolyte. Hildebrand solubility parameter is a square-root of intermolecular cohesive energy within a unit volume of material (unit = $MPa^{1/2}$) [40]. Solubility parameter is useful to predict the swelling behavior of polymers in solvents: Polymer swells more in a solvent with similar solubility parameter as the polymer. Solubility parameter is higher in polar solvent because of stronger dipole-dipole interaction. For example, solubility parameter of ethers ranges between 15 and 20 $MPa^{1/2}$ (e.g. diethyl ether = 15.8; 1, 4-dioxane = 20.5); linear carbonates range between 17 and 20 $MPa^{1/2}$ (e.g. DEC = 17.9; DMC = 19.4); cyclic carbonates range between 27 and 30 $MPa^{1/2}$ (e.g. PC = 27.3; EC = 29.6) [40,120]. Solubility parameters of polymer films used as protective coating of Li metal is listed in Table 2. Solubility parameters of some polymers have not been reported in literature. In this case, we listed the solubility parameter of the solvent which dissolves the polymer, since the solubility parameter of the polymer is expected to be similar to the value of the solvent.

Polymer materials are categorized into three types based on the solubility parameters: non-polar polymer (Section 7.1) with solubility parameter below 16 $MPa^{1/2}$; polar polymer (Section 7.2) with solubility parameter in the range of 20–25 $MPa^{1/2}$; strongly-polar polymer (Section 7.3) with solubility parameter above 26 $MPa^{1/2}$. A Polymer film swells and becomes ion-conductive only in a solvent with similar solubility parameter as the polymer. Therefore, non-polar polymer coating is usually used with less polar electrolyte such as ether electrolytes to maximize the film conductivity, except in the case the film has pores to let the solvent permeate through. Polar polymer films are conductive in both less-polar ether electrolyte, and polar carbonate electrolytes. Strongly-polar polymer films are only conductive in polar carbonate electrolytes. Chemical selectivity is generally observed in strongly-polar polymer, which is advantageous as a protective coating of Li metal (Section 2). For example, electrostatic interaction between Li^+ and sulfonate group enables a selective conduction of Li^+ through Nafion film (Section 7.3.1). Dipole-dipole interaction between EC and nitrile group of PAN reduces the reactivity of EC with Li metal (Section 7.3.2). On the other hand, polar group is generally at high oxidation state and therefore tends to be reduced by Li metal. Addition of a designed functional group to the polymer backbone which can form a stable SEI layer on Li metal can mitigate decomposition of both the coating layer and the electrolyte (Section 7.2.5-6).

Inorganic components such as LiF, Al_2O_3, L_3PS_4, or GO can be mixed with polymers to increase the mechanical strength of the protective layer. High shear modulus of inorganic compounds can suppress the dendrite growth (Section 2). In polymer/inorganic composite film, the polymer matrix glues the inorganic components together to enhance the film elasticity. Uniform distribution of the inorganic components, and the higher degree of bonding between the inorganic and polymer phases are the important conditions to realize uniform current distribution through the film.

CE of Li plating/stripping on polymer-coated Cu or inert metal electrode (e.g. stainless steel) are summarized in Table 2. High CE over 99% in a carbonate electrolyte was reported recently, which makes polymer or polymer/inorganic composite a promising material for stabilization of the electrolyte-Li interface.

7.1. Non-polar polymer

7.1.1. Poly(dimethyl siloxane)

PDMS is widely used because of the chemical stability against metallic Li, and the elastic property enables PDMS to form a thin film [125]. The protective function of PDMS film is often evaluated in an ether electrolyte consisting of DOL/DME as the mixed solvent, LiTFSI as the salt, and $LiNO_3$ as the additive. The ether electrolyte itself shows high CE without any coating layer (>98.5%) [126], and the efficiency with PDMS film in the ether electrolyte shows only limited enhancemnt.

Table 2
Conditions and CE of Li metal plating/stripping with various polymer or composite coatings on a flat working electrode. Note all electroplated Li metal is stripped at the end of each cycle. Solubility parameters of the solvent of the polymer are listed, in case the value of polymer is not available in literatures. Reference of solubility parameters: ref [121] for polymers, and ref [120] for solvents.

Material	Solubility parameter ($MPa^{1/2}$)	Coating method	Thickness	Electrolyte	Current (mA cm^{-2})	Capacity (mAh cm^{-2})	CE	Ref.
PDMS (dense)	15.5	Melt casting	1 μm	DOL/DME (1:1), 1 M LiTFSI, 1 wt % $LiNO_3$	1	1	97%	[54]
PDMS (porous)	15.5	Spin coating	500 nm	EC/DEC (1:1), 1 M $LiPF_6$	0.5	1	94.5%	[122]
PVDF-HFP + LiF	20.0 (acetone)	Solution casting	12 μm	DOL/DME (1:1) 1 M LiTFSI, 2% $LiNO_3$	0.5	1	97.2%	[66]
Poly(SF-DOL) + GO	20.3 (DCM)	Solution casting	3 μm	EC/EMC (3:7), 1 M $LiPF_6$, 2% LiBOB	1	1	99.3%	[22]
β-PVDF	23.2	Solution casting	4 μm	DOL/DME (1:1), 1 M LITFSI, 3 wt % $LiNO_3$	1	0.5	98%	[67]
Alucone	–	MLD	6 nm	DOL/DME (1:1), 1 M LiTFSI, 0.18 M Li_2S_8, 2% $LiNO_3$	0.4	1	99.5%	[44]
Poly(Imide-DOL)	24.8 (DMF)	Solution casting	2 μm	EC/EMC/FEC (3:7:1), 1 M $LiPF_6$	0.5	1	98.3%	[53]
PEDOT-PEO	25.1 (NM)	Spin coating	380 nm	EC/DMC (1:1), 1 M $LiClO_4$	–	–	–	[123]
PAN	26.1	Thermal crosslinking	40–200 μm	EC/DEC (1:3), 1 M $LiPF_6$	–	–	–	[124]
Li-Nafion + Al_2O_3	27.3 (PC)	Solution casting	200 nm	EC/DMC (1:1), 1 M $LiPF_6$, 10% FEC, 1% VC	3	3	92%	[21]
Polyurea	30.1	MLD	4 nm	EC/DEC/DMC (1:1:1), 1 M $LiPF_6$	–	–	–	[45]
Nafion	31 & 21	Spray coating	4 μm	EC/DEC (1:1), 1 M $LiPF_6$	–	–	–	[119]

Meanwhile, PDMS coating enables longer cycle life (>100 cycles) of Li deposition/stripping, compared to bare electrodes [54,127].

PDMS is a non-polar material and thus no Li salt can directly dissolve into this polymer [128]. The ion conduction through the PDMS layer must be mediated by the solvent molecules dissolved inside the film. PDMS film swells more in ether electrolytes, because the solubility parameter of PDMS (15.5 $MPa^{1/2}$) is closer to that of the ether electrolyte. In contrast, swelling ratio of PDMS is much lower in carbonate electrolytes, and thus the film is non-conductive. Zhu et al. reported a treatment of PDMS film with hydrofluoric acid (HF) creates nanopores to increase the ionic conductivity of PDMS film in carbonate electrolytes [122]. An average CE with the HF-treated PDMS film in a carbonate electrolyte (EC/DEC (1:1) + 1 M $LiPF_6$) reaches 94.5%.

Bao and Cui et al. studied flowable PDMS films, which can deform as Li dendrite grows [54]. Dynamic crosslinking between the polymer chains imparts fluid-like property to the coating layer and successfully suppress the dendritic growth of Li metal. With the flowable PDMS film coated on Cu electrode, the average CE achieves 97.0% over 100 cycles in an ether electrolyte (DOL/DME (1:1) + 1 M LiTFSI + 1 wt% $LiNO_3$) at 1 mA cm^{-2} and 1 mAh cm^{-2}. The authors also reported fluid-like polymer film made from polyamine [129]. Biased random walk simulation suggests that reduced ion conductivity in the fluid-like polymer coating may contribute to uniform deposition of Li metal [129].

Nazar et al. used PDMS as an elastic polymer support for Li_3PS_4 solid ion conductor [130]. Li_3PS_4 powder is cold pressed into a solid ion-conductive layer, and then the *in-situ* crosslinking among PDMS oligomers fills the void inside the Li_3PS_4 layer. An average CE of 95.8% over 200 cycles (1 mA cm^{-2}, 1 mAh cm^{-2}) is reported in an ether electrolyte with the Li_3PS_4-PDMS composite coating. While the presence of PDMS clearly improved the cycling stability, the moderate efficiency values indicate that significant electrolyte permeation takes place which reacts with lithium metal.

7.2. Polar polymers

7.2.1. Poly(vinylidene fluoride) and poly(vinylidene fluoride-co-hexafluoropropylene)

PVDF can react with Li metal to produce LiF at the interface. PVDF film contains both polar and non-polar phases, depending on the conformation of electronegative fluorine (F) atoms on the polymer chains: in α-phase, F atoms take alternating trans-gauche conformation with antiparallel dipole moments, and thus α-PVDF film exhibits nonpolar property; in β-phase, F atoms take all-trans conformation with parallel dipole moments, and thus β-PVDF film exhibits polar property. Wu et al. observed a flat deposition of Li metal on β-PVDF-coated Cu substrate, in contrast to the dendritic Li metal on bare Cu (Fig. 7a) [67]. The CE of Li plating in an ether electrolyte reaches 98% in the first 10 cycles on a copper electrode coated with polar β-PVDF film (Fig. 7b). Meanwhile, with the nonpolar α-PVDF coating, the initial CE begins from only 85% and then gradually improves to 98% after 200 cycles. The voltage hysteresis of polar β-PVDF coated copper is the same as the bare copper, while the hysteresis is doubled with non-polar α-PVDF coating. The polar β-PVDF film provides more conductive pathways to Li ion to diffuse through the polymer coating and plate underneath the coating layer.

PVDF-HFP is a highly fluorinated version of PVDF possessing trifluoro methane group. Because of uniform distribution of the dipole moment, PVDF-HFP is less polar than PVDF, and the surface energy is extremely low [131]. Huang et al. reported a composite film of PVDF-HFP and LiF microparticles to increase the mechanical strength of the polymer film [66]. The CE of Li deposition through the PVDF-HFP/LiF composite film in an ether electrolyte with $LiNO_3$ additive is 97.2%. Although the CE shows little increase from the bare Cu electrode, the protected Cu||Li cell cycles longer than the control cell (120 cycles).

7.2.2. Poly(3,4-ethylenedioxythiophene-co-ethylene oxide)

PEDOT is an electron-conductive polymer, while PEO is a Li^+-conductive polymer. The direct use of PEO (solubility parameter = 24.0 $MPa^{1/2}$, [121]) as the coating layer is not feasible due to its solubility in common organic electrolytes. Kim et al. reported the copolymer of PEDOT and PEO (PEDOT-*co*-EO), which is insoluble in organic electrolytes and strongly adheres to Li metal surface [123]. PEDOT-*co*-EO swells in a carbonate electrolyte (EC/DMC + 1 M $LiClO_4$) and shows high ionic conductivity (3.5×10^{-3} S cm^{-1}). The cycling life of Li||$LiCoO_2$ cell is increased when Li metal anode is coated with

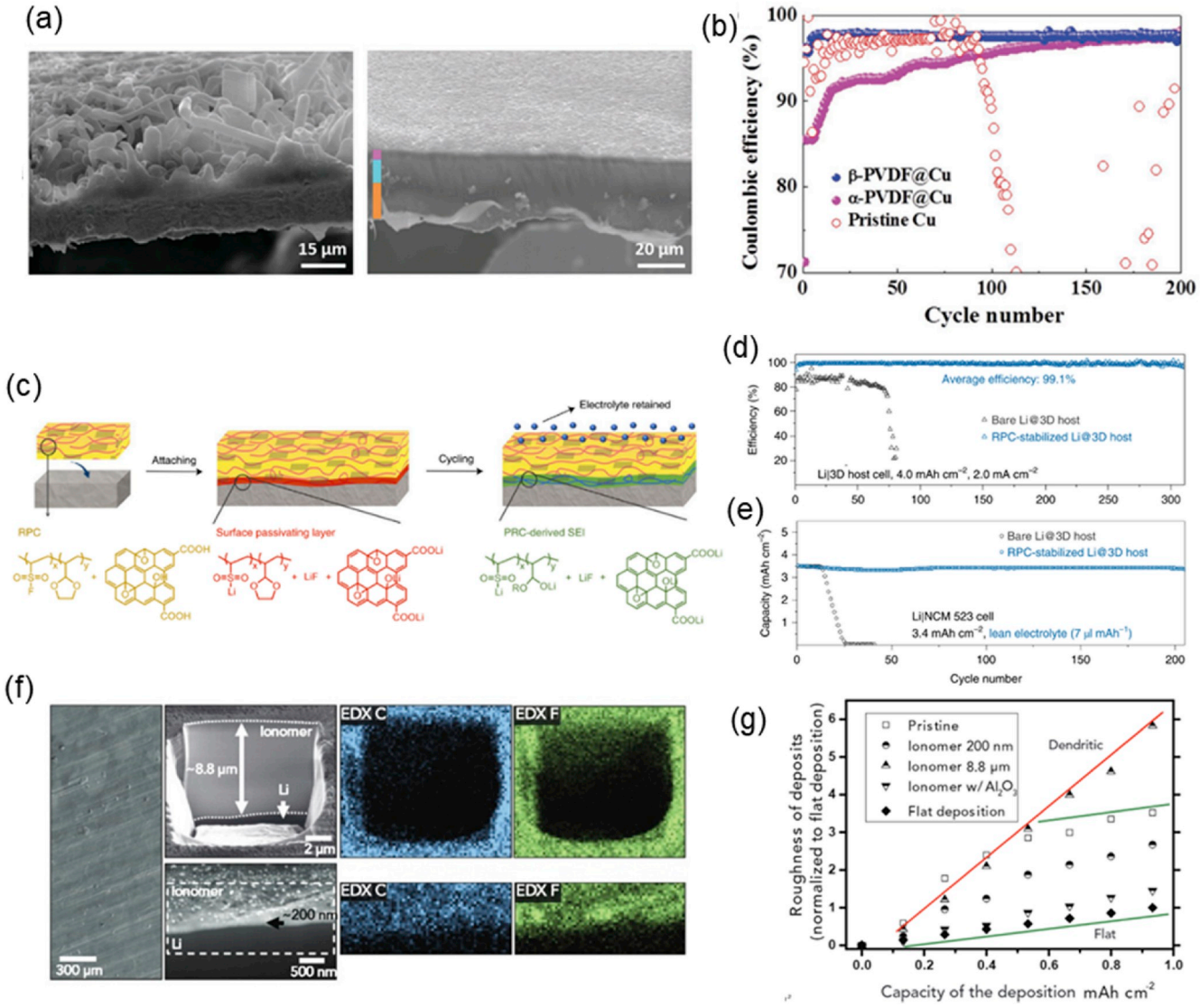

Fig. 7. (a) SEM images of copper surface after electrodeposition of Li metal (1 mA cm^{-2}, 2 mAh cm^{-2}) without coating (left) and with β-PVDF coating (right). (b) CE of Li metal plating/ stripping with polar β-PVDF coating; nonpolar α-PVDF coating; and without coating. Reproduced with permission. [67] Copyright 2017, John Wiley and Sons. (c) Formation of SEI layer after the application of reactive polymer coating (RPC consisting of poly(SF-DOL) and GO) on Li metal surface. (d) CE of RPC-stabilized Li metal deposited in 3D carbon host, and the comparison with uncoated 3D host (2 mA cm^{-2}, 4 mAh cm^{-2}). (e) Capacity retention of RPC-stabilized 3D Li ||NCM 523 full cell under lean electrolyte condition. Reproduced with permission. [22] Copyright 2019, Springer Nature. (f) Cross-sectional SEM images and EDX mappings of ionomer (Li-Nafion) coating at a thickness of 9 μm (top) and 200 nm (bottom). (g) Roughness of electroplated Li metal at various deposition capacity. Reproduced with permission. [21] Copyright 2017, Elsevier.

PEDOT-*co*-EO coating. Kim et al. also incorporated AlF_3 particles in PEDOT-*co*-EO to form a composite coating [132]. AlF_3 is expected to serve as a solid component to mechanically suppress growth of the Li dendrite. As a result, the voltage polarization is reduced by this composite coating, and also cycling life of a Li||O_2 cell is extended.

7.2.3. *Alucone*

Alucone is a hybrid metal-organic material where ethylene oxide units are bridged by aluminum cation. Alucone is directly grown from Li metal surface by MLD with trimethyl aluminum and ethylene glycol as the precursors. Elam et al. reported that the Li||Li cycling life is enhanced in a carbonate electrolyte with 6-nm-thick alucone coating [44]. The morphology of electrodeposited Li is denser with the alucone coating, however, no significant increase of the CE was observed despite a longer cycling life compared to the control cell.

7.2.4. *Poly((N-2,2-dimethyl-1,3-dioxolane-4-methyl)-5-norbornene-exo-2,3-dicarboximide)*

Ether-based organic electrolyte is known to show better cycle life for Li metal compared to carbonate electrolyte. This exceptional stability is believed to be the result of decomposition of ether solvents on the Li surface to form polymeric SEI layers. Wang et al. designed a copolymer, poly(Imide-DOL), where a DOL is attached to a norbornene-*exo*-dicarboximide main chain [53]. The cyclic ether group decomposes on Li surface to produce ether-based SEI layer, while the rigid cyclic carboximide group imparts stiffness to the entire film. A moderate degree of polymer swelling in carbonate electrolytes provides ionic conductivity to the polymer film. The CE of Li deposition/dissolution with this polymer coating is increased to 98.3% over 200 cycles in a carbonate electrolyte with FEC as the additive (EC/EMC/FEC (3:7:1) + 1 M $LiPF_6$). This efficiency is close to the value of ether electrolytes.

7.2.5. Poly(vinyl sulfonyl fluoride-ran-2-vinyl-1,3-dioxolane)

Wang et al. also reported another type of copolymer, poly(SF-DOL) composed of DOL, and sulfonyl fluoride (-SO_2F, SF) groups [22]. SF group is reduced on the lithium surface to produce LiF as the SEI component (Fig. 7c). GO nanosheets is mixed into the polymer layer to further enhance the interface stability. This polymer/GO coating is named as reactive polymer coating (RPC) after the designed reactivity with Li metal. CE of Li metal deposition on a flat stainless-steel electrode achieves 99.3% at 1 mA cm^{-2} and 1 mAh cm^{-2} in a carbonate electrolyte (EC/EMC/FEC (3:7:1) + 1 M $LiPF_6$ + 2%LiBOB). Poly(SF-DOL) coating is applied on a carbon-based 3D host, and the CE achieves 99.1% at high current density (2.0 mA cm^{-2}) and high capacity (4.0 mAh cm^{-2}) (Fig. 7d). Poly(SF-DOL)-coated 3D host can be lithiated to form Li-containing anode and paired with NCM 523 cathode. Impressively, under limited amount of Li metal (1.9-fold excess) plated inside the RPC-protected 3D host, and limited volume of electrolyte (7 μm mAh^{-1}), the Li||NCM 523 cell retained 90% of the initial capacity after 200 cycles (Fig. 7e).

7.3. Strongly-polar polymer

7.3.1. Nafion

Nafion is an ionomer where sulfonate group is tethered onto PTFE backbone. Nafion has two solubility parameters, 21 $MPa^{1/2}$ (attributed to the PTFE backbone) and 31 M $Pa^{1/2}$ (attributed to the ionic sulfonate group) [133]. By exchanging H^+ on sulfonate group to Li^+ (Li-Nafion), Li-Nafion selectively conducts Li^+ through the ionic cluster formed at sulfonate group (i.e. high transference number of Li^+).

Kim et al. laminated 4 μm-thick Nafion layer on Li metal as the protective coating and used in a carbonate electrolyte (EC/DEC + 1 M $LiPF_6$) [119]. FTIR spectroscopy on the Nafion film confirms ion exchange between H^+ and Li^+ takes place during Li plating/stripping. Nafion coating on Li metal maintains smooth surface after 10 cycles of Li||Li cycling at high current density (10 mA cm^{-2}, 4 mAh cm^{-2}), showing the good mechanical stability of Nafion. Under the same condition, Nafion-coated Li metal can be cycled for 250 cycles (2000 h in total). The authors compared the Li||Li cycling result with 50 μm-thick Li-Nafion. The thick Li-Nafion film shows transference number of Li^+ (t_{Li+}) close to unity, which is higher than 4 μm-thick Nafion film (where t_{Li+} = 0.83). However, the conductivity of thick Nafion is one-order lower (3.33×10^{-6} S cm^{-1}) than 4 μm-thick Nafion layer (1.42×10^{-5} S cm^{-1}). Low ionic conductivity of thick Nafion film resulted in unstable voltage curves and large polarizations in galvanostatic Li||Li cycling, and the cell failed at low current density of 0.2 mA cm^{-2}. The deposited Li metal underneath the thick Nafion film is patchy and dendritic. This comparison experiment highlights the importance of high ionic conductivity of polymer film for depositing Li in uniform and smooth morphology.

Archer et al. dissolved ion-exchanged Li-Nafion in PC and solution-casted on Li metal to form 200 nm-thick Li-Nafion film (Fig. 7f) [21]. The Li-Nafion film prepared by this method is even thinner than the film used by Kim et al. [119] and therefore shows higher ionic conductivity (2×10^{-3} S cm^{-1}), while maintaining high transference number of Li^+ (t_{Li+} = 0.88). Additionally, nanoporous Al_2O_3 membrane (20 nm pore size) were combined with the Li-Nafion layer to increase the mechanical strength of the composite coating. In a carbonate electrolyte (EC/DMC (1:1) + 1 M $LiPF_6$), the roughness of Li metal deposited under the 200 nm-thick Li-Nafion/Al_2O_3layer is close to the value of flat deposition (Fig. 7g). On the contrary, the Li dendrites are observed when 9-μm-thick Li-Nafion coating is used. This result agrees with the observation by Kim et al. [119]. Because thick Nafion film shows only limited ionic conductivity, Li metal preferentially grows from the defect sites in the polymer film and eventually breaks the coating layer. With a thinner coating with higher ionic conductivity, the ion transport is not hindered and Li deposits underneath the coating layer.

In mixed carbonate electrolyte (EC/DMC + 1 M $LiPF_6$ + 10% FEC + 1% VC), the CE of Li plating/striping is improved from 86% with pristine Li counter electrode to 92% with Li-Nafion/Al_2O_3-protected Li counter electrode (0.5 mA cm^{-2}/1 mAh cm^{-2}). Similar CE is observed under higher current density and capacity (3 mA cm^{-2}, 3 mAh cm^{-2}).

7.3.2. Polyacrylonitrile

EC is less stable in contact with Li metal and susceptible to the decomposition reaction compared to ether solvents. Nevertheless, oxidative stability of EC makes it compatible with 4V-cathode. To enhance the reduction-stability of EC with Li metal, Yu et al. recently developed a PAN-based polymer gel film [124]. The film was prepared by thermal crosslinking of PEGDA oligomer mixed in a polymer solution of PAN, EC, and LiTFSI. Dipole-dipole interaction between C≡N group of PAN and C═O group of EC increases the energy level of lowest unoccupied molecular orbital (LUMO) and makes EC resistant toward reduction. FTIR, and Raman spectroscopy on PAN-PEGDA-EC-LiTFSI gel film evidences a coordination between PAN and EC, and decreased number of free EC molecules, respectively. The PAN-gel-protected Li shows stable Li||Li cycling at 10 mA cm^{-2} and 1 mAh cm^{-2} for 100 cycles. The cycled Li is shiny, and SEM shows densely deposited Li. Although CE of Li plating/stripping is not reported, Li||NCM 111 cell shows good capacity retention of 94.0% after 450 cycles at 1C rate.

7.3.3. Polyurea

Polyurea film can be directly coated on a Li foils by the MLD technique with ethylenediamine and 1,4-phenylene diisocyanate as the precursors [45]. The growth rate of the film is controlled by the number of reaction cycle, and the typical growth rate is 0.4 nm per cycle. Amide bonding in polyurea makes the film polar, which in turn regulates the ion flux of Li cation. Hildebrand solubility parameter of poly(*N*-methacryl urea) is reported as 30.7 $MPa^{1/2}$, which is close to the value of EC [121]. Sun et al. reported that 4 nm-thick polyurea coating enables stable Li||Li cycling in a carbonate electrolyte (EC/DEC/DMC (1:1:1) + 1 M $LiPF_6$) at 3 mA cm^{-2} and 1 mAh cm^{-2} for 200 h [45].

8. Summary and future perspectives

The past few years have witnessed a large variety of protective coatings made of both inorganic and polymeric materials that have been reported to give better cycling performance than bare Li metal in either Li||Li symmetric cycling or CE tests. In order for the protective coating approach to help enable Li metal anode to achieve efficiencies of >99.72% (CE is calculated based on the cell requirement for practical Li metal battery [1]) and ultimately a 500 Wh kg^{-1} lithium metal battery, we advocate for several research directions that merit attention from the research community.

8.1. Ion conduction mechanism through the coating layer

Ion conduction is an inherently complex issue for a thin coating layer. For example, a layer of solid ion conductor immersed in liquid electrolyte offers two pathways of ion conduction either through the solid phase, the liquid phase, or both. If the solid conductive layer has no porosity and is also free from any defect, the ion conduction is only possible through the solid phase. However, when the solid conductive layer possesses inherent defects or porosity, permeation of the liquid electrolyte through the pores is possible. In this case, ion conduction through the liquid phase is more probable, because the ionic conductivity of liquid phase is generally higher than solid phase. Although permeation of the liquid electrolyte into the solid phase may increase the overall ionic conductivity of the protective coating, the selectivity towards Li ion inevitably decreases, leading to increasing rate of side reactions with the leaked electrolyte. Therefore, evaluation of the respective ion conductivity in the liquid and the solid phases, by AC impedance technique for example [39], is essential to understand the ion conduction mechanism and to improve the design of protective

coatings. Similarly, evaluation of swelling behavior of polymeric coatings in the liquid electrolyte, the resulting ionic conductivity, and the selectivity toward Li ion (i.e. transference number) should be studied in detail. A correlation between the dielectric constant of polymers and the size of Li metal nuclei can aid understanding on the electroplating behavior of Li metal through polymer coatings [134].

8.2. Mechanistic understanding of protection layer degradation

Mechanical toughness of the protective coatings should be studied after long cycles of Li plating/stripping. Growing Li metal deposits under the coating layer creates stress and can eventually break the coating. As-formed defect becomes a local hotspot promoting more deposition of Li metal. The local defect in 9-μm-thick Li-Nafion layer promoted dendritic growth of Li metal due to the high current density localized at the defect point (Section 7.3.1) [21]. In contrast, the cracks in 15-nm-thick LiPON layer resulted in a flat deposition of Li metal growing on top of the LiPON layer (Section 6.2.1) [92]. Therefore, the improved performance in Li||Li cycling or CE tests may have little relation with the protection mechanisms (i.e. mechanical suppression and chemical selectivity), when the coating layer is fractured during the electroplating. Possibly, when Li metal grows on top of the protective layer, a highly lithiophilic coating layer may promote a flat deposition.

8.3. Evaluation of coating layer performance under practical conditions and cell configurations for high energy density

Here, we discuss the practical testing conditions for protective coatings aiming for the high energy density of 500 Wh kg^{-1} [1]. In literature, the specific capacity of Li metal is often claimed as 3860 mAh g^{-1}, however, the excess amount of Li metal on the anode side diminishes the effective capacity of Li metal (Fig. 8a). For example, the effective specific capacity of Li metal anode with 50%, 500%, 5000% excess Li metal drops to 2570, 640, 76 mAh g^{-1}, respectively. The effect of coating layers on thin (less excess) Li metal surface needs to be evaluated to claim the high energy density of Li metal. The CE can be evaluated in a practical cell configuration by pairing cathode with thin Li metal (Section 5.4). Capacity retention versus cycle number with 40% excess Li metal is simulated at varied CE of Li plating/stripping (Fig. 8b). In the plateau region, the excess Li metal is consumed, and then the capacity starts decaying in an exponential manner after all the excess Li is consumed. The 0.2% increase in the CE from 99.6% to 99.8% doubles the cycle life of the plateau region. Recently, increasing number of studies on anode free battery (0% excess Li) and thin-Li metal battery has been published [80,126,135,136]. For example, 83% of capacity retention of thin-Li||LFP battery after 100 cycles was demonstrated by Zhou et al. [135] The CE of Li metal anode is evaluated as 99.3% under 0.2 mA cm^{-2} with 0.8 mAh cm^{-2} of capacity in their study.

Reduction of the amount of liquid electrolyte used in the battery cell is an effective pathway to increasethe energy density (Fig. 8d). However, the cycle life of Li metal battery significantly deteriorates under limited amount of electrolyte [1]. Electrolyte is consumed during the battery cycling by the formation of SEI layer and porous Li metal. This sponge-like Li metal with high surface area accelerates the consumption rate of liquid electrolyte to cause the electrolyte depletion. The high porosity then requires greater volume of electrolyte to maintain normal battery operation. Applying a protective coating layer on Li metal is a promising strategy to reduce the rate of electrolyte consumption under lean electrolyte condition.

In recent studies on Li metal anode, the shape of current collector is modified from conventional 2D planar structure to 3D porous scaffold to accommodate the volume expansion of Li metal and simultaneously to reduce the amount of isolated Li particles from the current collector [13–16]. Application of the protective coatings on such 3D scaffold or host is highly anticipated to boost the CE of Li plating (Fig. 8e). As a proof of concept, Wang et al. recently reported 200 cycles of Li||NCM 523 full cell with limited volume of electrolyte and 90%-excess Li plated on polymer-protected 3D carbon scaffold (Section 7.2.5) [22].

The CE of Li metal anode has been steadily increasing thanks to the recent development of high-efficiency electrolytes. The compatibility of such electrolytes with high voltage cathode, for example NMC 811, is also demonstrated [80,137]. The electrolyte contains highly-fluorinated

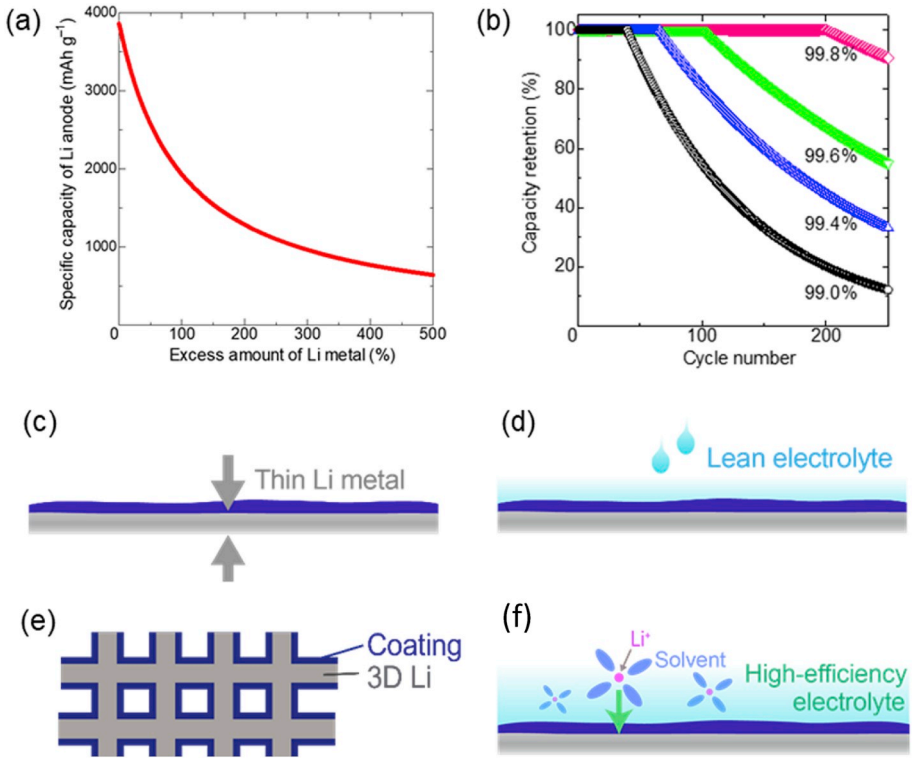

Fig. 8. (a) Drop of specific capacity of Li metal anode with increasing amount of excess Li metal. 0% excess Li means all Li^+ ions transfer between the anode and the cathode during charging/discharging. (b) Simulated capacity retention of Li metal battery with 40% excess amount of Li metal with increasing CE of the Li anode. Capacity loss at the cathode side is assumed to be negligibly small compared to the anode side. Prospective testing conditions for Li metal anode with the protective coatings: (c) Thin Li metal electrode to reduce the excess amount of Li; (d) Lean electrolyte to reduce the total weight of the battery pack; (e) Coating on the 3D-structured Li metal to reduce the influence of volume change during plating/stripping of Li metal; (f) Protective coating used with state-of-the-art electrolyte to further increase the CE of Li metal anode.

ether or carbonate solvents to form a robust SEI layer on Li metal surface. The challenge in the studies of electrolyte is still to realize the CE of Li metal anode above 99.7%. Interesting future studies would be the combination of protective coatings and state-of-the-art electrolytes to increase the upper limit of the CE (Fig. 8f). Finally, more studies on the cell-level engineering to solve safety issues of liquid electrolyte based Li metal battery will be necessary in conjunction with increasing CE of Li metal anode [34,138,139].

Declaration of competing interest

The authors declare that they have no known competing financial interests or personal relationships that could have appeared to influence the work reported in this paper.

Acknowledgment

This work was supported by the Office of Vehicle Technologies of the U.S. Department of Energy through the Advanced Battery Materials Research (BMR) Program (Battery500 Consortium) under Contract No. DE-EE0007764.

Abbreviation Full name

AC	alternate current
AFM	atomic force microscopy
Al_2O_3	aluminum oxide
ALD	atomic layer deposition
AlF_3	aluminum trifluoride
ATR	attenuated total reflectance
C_2Cl_4	perchloroethylene
CE	coulombic efficiency
CNT	carbon nanotube
cryo	cryogenic-temperature
Cu||Li	two-electrode cell with copper as working and lithium metal as reference and counter electrodes
DCM	dichloromethane
DEC	diethyl carbonate
DMC	dimethyl carbonate
DMC	dimethyl carbonate
DME	dimethoxyethane
DME	dimethyl ether
DMF	N,N′-dimethyl formamide
DOL	1,3-dioxolane
EC	ethylene carbonate
ED	electron diffraction
EDX	energy dispersive X-ray
EELS	electron energy-loss spectroscopy
EIS	electrochemical impedance spectroscopy
EMC	ethyl methyl carbonate
FEC	fluoroethylene carbonate
FTIR	Fourier transform infrared spectroscopy
GF	fluorinated graphene
GO	graphene oxide
HF	hydrogen fluoride
LFP	lithium iron phosphate ($LiFePO_4$)
Li	lithium
Li||Li	two-electrode cell with lithium metal at both sides
Li_2CO_3	lithium carbonate
Li_2O	lithium oxide
Li_2S	lithium disulfide
Li_2S_6	dilithium hexasulfide
Li_3P	lithium phosphide
Li_3PO_4	lithium phosphate
Li_3PS_4	lithium phosphorous sulfide
LiBOB	lithium bis(oxalato)borate
LiCl	lithium chloride
$LiClO_4$	lithium perchlorate
LiF	lithium fluoride
LiI	lithium iodide
Li-Nafion	lithiated Nafion
$LiNO_3$	lithium nitrate
LiOH	lithium hydroxide
$LiPF_6$	lithium hexafluorophosphate
LiPON	lithium phosphorous oxynitride
LiTFSI	lithium bis(trifluoromethanesulfonyl)imide
LLCZN	$Li_7La_{2.75}Ca_{0.25}Zr_{1.75}Nb_{0.25}O_{12}$
LLZO	$Li_7La_3Zr_2O_{12}$
LMC	lithium methyl carbonate
LP30	commercial electrolyte composed of EC:DMC = 1:1 + 1 M $LiPF_6$
MLD	molecular layer deposition
MoS_2	molybdenum disulfide
MPS	3-mercaptopropyl trimethoxysilane
NCA	$LiNi_{0.8}Co_{0.15}Al_{0.05}O_2$
NCM 523	$LiNi_{0.5}Co_{0.2}Mn_{0.3}O_2$
NM	nitromethane
NMC	lithium nickel manganese oxide ($LiNi_{1-x-y}Mn_xCo_yO_2$)
NMC 111	$LiNi_{1/3}Co_{1/3}Mn_{1/3}O_2$
NMC811	$LiNi_{0.8}Mn_{0.1}Co_{0.1}O_2$
NMP	N-methyl-2-pyrrolidone
P_2S_5	diphosphorous pentasulfide
PAN	polyacrylonitrile
PC	propylene carbonate
PCl_3	phosphorous trichloride
PDMS	polydimethyl siloxane
PEDOT	poly(3,4-ethylenedioxythiophene)
PEGDA	polyethylene glycol diacrylate
PEO	poly(ethylene oxide)
PFT	peak force tapping
poly(Imide-DOL)	poly((*N*-2,2-dimethyl-1,3-dioxolane-4-methyl)-5-norbornene-*exo*-2,3-dicarboximide)
poly(SF-DOL)	poly(vinyl sulfonyl fluoride-*ran*-2-vinyl-1,3-dioxolane)
PTFE	tetrafluoroethylene
PTMEG	poly(tetrametylene ether glycol
PVDF	polyvinylidene fluoride
PVDF-HFP	polyvinylidene fluoride-*co*-hexafluoropropylene
QCM	quartz crystal microbalance
Q_p	capacity obtained after complete plating of Li metal on Cu electrode
Q_s	capacity obtained after complete stripping of Li metal from Cu electrode
RPC	reactive polymer coating
sat	saturated
SEI	solid electrolyte interface
SEM	scanning electron microscopy
SF	sulfonyl fluoride, $-SO_2F$ group
$SnCl_4$	tin tetrachloride
STEM	scanning transmission microscopy
t-BuOLi	lithium *tert*-buthoxide
TEM	transmission electron microscopy
TEOS	tetraethoxysilane
THF	tetrahydrofurane
t_{Li+}	transference number of Li^+
VC	vinylene carbonate
XPS	X-ray photoelectronic spectroscopy
XRD	X-ray diffraction
ZnO	zinc oxide

References

[1] J. Liu, Z. Bao, Y. Cui, E.J. Dufek, J.B. Goodenough, P. Khalifah, Q. Li, B.Y. Liaw, P. Liu, A. Manthiram, Y.S. Meng, V.R. Subramanian, M.F. Toney, V. V. Viswanathan, M.S. Whittingham, J. Xiao, W. Xu, J. Yang, X.-Q. Yang, J.-G. Zhang, Pathways for practical high-energy long-cycling lithium metal batteries, Nat. Energy. 4 (2019) 180–186, https://doi.org/10.1038/s41560-019-0338-x.

[2] X. Cheng, R. Zhang, C. Zhao, Q. Zhang, Toward safe lithium metal anode in rechargeable Batteries : a review, Chem. Rev. 117 (2017) 10403–10473, https://doi.org/10.1021/acs.chemrev.7b00115.

[3] C. Niu, H. Lee, S. Chen, Q. Li, J. Du, W. Xu, J.G. Zhang, M.S. Whittingham, J. Xiao, J. Liu, High-energy lithium metal pouch cells with limited anode swelling and long stable cycles, Nat. Energy. 4 (2019) 551–559, https://doi.org/10.1038/s41560-019-0390-6.

[4] S.S. Zhang, Problem, status, and possible solutions for lithium metal anode of rechargeable batteries, ACS Appl. Energy Mater. 1 (2018) 910–920, https://doi.org/10.1021/acsaem.8b00055.

[5] C. Fang, J. Li, M. Zhang, Y. Zhang, F. Yang, J.Z. Lee, M.-H. Lee, J. Alvarado, M. A. Schroeder, Y. Yang, B. Lu, N. Williams, M. Ceja, L. Yang, M. Cai, J. Gu, K. Xu, X. Wang, Y.S. Meng, Quantifying inactive lithium in lithium metal batteries, Nature 572 (2019) 511–515, https://doi.org/10.1038/s41586-019-1481-z.

[6] Z. Zeng, V. Murugesan, K.S. Han, X. Jiang, Y. Cao, L. Xiao, X. Ai, H. Yang, J. G. Zhang, M.L. Sushko, J. Liu, Non-flammable electrolytes with high salt-to-solvent ratios for Li-ion and Li-metal batteries, Nat. Energy. 3 (2018) 674–681, https://doi.org/10.1038/s41560-018-0196-y.

[7] J. Alvarado, M.A. Schroeder, T.P. Pollard, X. Wang, J.Z. Lee, M. Zhang, T. Wynn, M. Ding, O. Borodin, Y.S. Meng, K. Xu, Bisalt ether electrolytes: a pathway towards lithium metal batteries with Ni-rich cathodes, Energy Environ. Sci. 12 (2019) 780–794, https://doi.org/10.1039/c8ee02601g.

[8] L. Yu, S. Chen, H. Lee, L. Zhang, M.H. Engelhard, Q. Li, S. Jiao, J. Liu, W. Xu, J. G. Zhang, A localized high-concentration electrolyte with optimized solvents and lithium difluoro(oxalate)borate additive for stable lithium metal batteries, ACS Energy Lett 3 (2018) 2059–2067, https://doi.org/10.1021/acsenergylett.8b00935.

[9] W. Li, H. Yao, K. Yan, G. Zheng, Z. Liang, Y.M. Chiang, Y. Cui, The synergetic effect of lithium polysulfide and lithium nitrate to prevent lithium dendrite growth, Nat. Commun. 6 (2015) 7436, https://doi.org/10.1038/ncomms8436.

[10] G. Li, Q. Huang, X. He, Y. Gao, D. Wang, S.H. Kim, D. Wang, Self-formed hybrid interphase layer on lithium metal for high-performance lithium-sulfur batteries, ACS Nano 12 (2018) 1500–1507, https://doi.org/10.1021/acsnano.7b08035.

[11] P.J. Kim, V.G. Pol, High performance lithium metal batteries enabled by surface tailoring of polypropylene separator with a polydopamine/graphene layer, Adv. Energy Mater. 8 (2018) 1802665, https://doi.org/10.1002/aenm.201802665.

[12] Y. Liu, Q. Liu, L. Xin, Y. Liu, F. Yang, E.A. Stach, J. Xie, Making Li-metal electrodes rechargeable by controlling the dendrite growth direction, Nat. Energy. 2 (2017) 17083, https://doi.org/10.1038/nenergy.2017.83.

[13] H. Liu, X. Yue, X. Xing, Q. Yan, J. Huang, V. Petrova, H. Zhou, P. Liu, A scalable 3D lithium metal anode, Energy Storage Mater. 16 (2019) 505–511, https://doi.org/10.1016/j.ensm.2018.09.021.

[14] J. Xie, J. Wang, H.R. Lee, K. Yan, Y. Li, F. Shi, W. Huang, A. Pei, G. Chen, R. Subbaraman, J. Christensen, Y. Cui, Engineering stable interfaces for three-dimensional lithium metal anodes, Sci. Adv. 4 (2018), https://doi.org/10.1126/sciadv.aat5168 eaat5168.

[15] K.H. Chen, A.J. Sanchez, E. Kazyak, A.L. Davis, N.P. Dasgupta, Synergistic effect of 3D current collectors and ALD surface modification for high coulombic efficiency lithium metal anodes, Adv. Energy Mater. 9 (2019) 1802534, https://doi.org/10.1002/aenm.201802534.

[16] C. Niu, H. Pan, W. Xu, J. Xiao, J.G. Zhang, L. Luo, C. Wang, D. Mei, J. Meng, X. Wang, Z. Liu, L. Mai, J. Liu, Self-smoothing anode for achieving high-energy lithium metal batteries under realistic conditions, Nat. Nanotechnol. 14 (2019) 594–601, https://doi.org/10.1038/s41565-019-0427-9.

[17] R. Weber, M. Genovese, A.J. Louli, S. Hames, C. Martin, I.G. Hill, J.R. Dahn, Long cycle life and dendrite-free lithium morphology in anode-free lithium pouch cells enabled by a dual-salt liquid electrolyte, Nat. Energy. 4 (2019) 683–689, https://doi.org/10.1038/s41560-019-0428-9.

[18] M. Genovese, A.J. Louli, R. Weber, S. Hames, J.R. Dahn, Measuring the Coulombic efficiency of lithium metal cycling in anode-free lithium metal batteries, J. Electrochem. Soc. 165 (2018) A3321–A3325, https://doi.org/10.1149/2.0641814jes.

[19] Q. Cheng, L. Wei, Z. Liu, N. Ni, Z. Sang, B. Zhu, W. Xu, M. Chen, Y. Miao, L. Q. Chen, W. Min, Y. Yang, Operando and three-dimensional visualization of anion depletion and lithium growth by stimulated Raman scattering microscopy, Nat. Commun. 9 (2018) 2942, https://doi.org/10.1038/s41467-018-05289-z.

[20] M.D. Tikekar, S. Choudhury, Z. Tu, L.A. Archer, Design principles for electrolytes and interfaces for stable lithium-metal batteries, Nat. Energy. 1 (2016) 16114. https://doi.org/10.1038/nenergy.2016.114.

[21] Z. Tu, S. Choudhury, M.J. Zachman, S. Wei, K. Zhang, L.F. Kourkoutis, L. A. Archer, Designing artificial solid-electrolyte interphases for single-ion and high-efficiency transport in batteries, Joule 1 (2017) 394–406, https://doi.org/10.1016/j.joule.2017.06.002.

[22] Y. Gao, Z. Yan, J.L. Gray, X. He, D. Wang, T. Chen, Q. Huang, Y.C. Li, H. Wang, S. H. Kim, T.E. Mallouk, D. Wang, Polymer–inorganic solid–electrolyte interphase for stable lithium metal batteries under lean electrolyte conditions, Nat. Mater. 18 (2019) 384–389, https://doi.org/10.1038/s41563-019-0305-8.

[23] D. Lin, Y. Liu, Y. Cui, Reviving the lithium metal anode for high-energy batteries, Nat. Nanotechnol. 12 (2017) 194–206, https://doi.org/10.1038/nnano.2017.16.

[24] X.Q. Zhang, X.B. Cheng, Q. Zhang, Advances in interfaces between Li metal anode and electrolyte, Adv. Mater. Interfaces. 5 (2018) 1701097, https://doi.org/10.1002/admi.201701097.

[25] R. Xu, X.-B. Cheng, C. Yan, X.-Q. Zhang, Y. Xiao, C.-Z. Zhao, J.-Q. Huang, Q. Zhang, Artificial interphases for highly stable lithium metal anode, Matter 1 (2019) 317–344, https://doi.org/10.1016/j.matt.2019.05.016.

[26] C. Monroe, J. Newman, The effect of interfacial deformation on electrodeposition kinetics, J. Electrochem. Soc. 151 (2004) A880, https://doi.org/10.1149/1.1710893.

[27] C. Monroe, J. Newman, The impact of elastic deformation on deposition kinetics at lithium/polymer interfaces, J. Electrochem. Soc. 152 (2005) A396, https://doi.org/10.1149/1.1850854.

[28] S. Yu, R.D. Schmidt, R. Garcia-Mendez, E. Herbert, N.J. Dudney, J.B. Wolfenstine, J. Sakamoto, D.J. Siegel, Elastic properties of the solid electrolyte Li7La3Zr2O12 (LLZO), Chem. Mater. 28 (2016) 197–206, https://doi.org/10.1021/acs.chemmater.5b03854.

[29] H.Z. Geng, R. Rosen, B. Zheng, H. Shimoda, L. Fleming, J. Liu, O. Zhou, Fabrication and properties of composites of poly(ethylene oxide) and functionalized carbon nanotubes, Adv. Mater. 14 (2002) 1387–1390, https://doi.org/10.1002/1521-4095(20021002)14:19<1387::AID-ADMA1387>3.0.CO;2-Q.

[30] P. Barai, K. Higa, V. Srinivasan, Lithium dendrite growth mechanisms in polymer electrolytes and prevention strategies, Phys. Chem. Chem. Phys. 19 (2017) 20493–20505, https://doi.org/10.1039/c7cp03304d.

[31] S. Wei, Z. Cheng, P. Nath, M.D. Tikekar, G. Li, L.A. Archer, Stabilizing electrochemical interfaces in viscoelastic liquid electrolytes, Sci. Adv. 4 (2018), https://doi.org/10.1126/sciadv.aao6243 eaao6243.

[32] M.D. Tikekar, G. Li, L.A. Archer, D.L. Koch, Electroconvection and morphological instabilities in potentiostatic electrodeposition across liquid electrolytes with polymer additives, J. Electrochem. Soc. 165 (2018) A3697–A3713, https://doi.org/10.1149/2.0271816jes.

[33] Q. Zhao, X. Liu, S. Stalin, K. Khan, L.A. Archer, Solid-state polymer electrolytes with in-built fast interfacial transport for secondary lithium batteries, Nat. Energy. 4 (2019) 365, https://doi.org/10.1038/s41560-019-0349-7.

[34] H. Zhou, H. Liu, Y. Li, X. Yue, X. Wang, M. Gonzalez, Y.S. Meng, P. Liu, In situ formed polymer gel electrolytes for lithium batteries with inherent thermal shutdown safety features, J. Mater. Chem. A. 7 (2019) 16984–16991, https://doi.org/10.1039/c9ta02341k.

[35] R.J. Blint, Binding of ether and carbonyl oxygens to lithium ion, J. Electrochem. Soc. 142 (1995) 696–702, https://doi.org/10.1149/1.2048519.

[36] C.M. Tenney, R.T. Cygan, Analysis of molecular clusters in simulations of lithium-ion battery electrolytes, J. Phys. Chem. C 117 (2013) 24673–24684, https://doi.org/10.1021/jp4039122.

[37] G. Yang, I.N. Ivanov, R.E. Ruther, R.L. Sacci, V. Subjokova, D.T. Hallinan, J. Nanda, Electrolyte solvation structure at solid/liquid interface probed by nanogap surface-enhanced Raman spectroscopy, ACS Nano 12 (2018) 10159–10170, https://doi.org/10.1021/acsnano.8b05038.

[38] Y. Yamada, F. Sagane, Y. Iriyama, T. Abe, Z. Ogumi, Kinetics of lithium-ion transfer at the interface between Li 0.35La0.55TiO3 and binary electrolytes, J. Phys. Chem. C 113 (2009) 14528–14532, https://doi.org/10.1021/jp9043539.

[39] M.R. Busche, T. Drossel, T. Leichtweiss, D.A. Weber, M. Falk, M. Schneider, M. L. Reich, H. Sommer, P. Adelhelm, J. Janek, Dynamic formation of a solid-liquid electrolyte interphase and its consequences for hybrid-battery concepts, Nat. Chem. 8 (2016) 426–434, https://doi.org/10.1038/nchem.2470.

[40] J.N. Lee, C. Park, G.M. Whitesides, Solvent compatibility of poly (dimethylsiloxane)-based microfluidic devices, Anal. Chem. 75 (2003) 6544–6554, https://doi.org/10.1021/ac0346712.

[41] S.M. George, Atomic layer deposition: an overview, Chem. Rev. 110 (2010) 111–131, https://doi.org/10.1021/cr900056b.

[42] L. Chen, K.S. Chen, X. Chen, G. Ramirez, Z. Huang, N.R. Geise, H.G. Steinrück, B. L. Fisher, R. Shahbazian-Yassar, M.F. Toney, M.C. Hersam, J.W. Elam, Novel ALD chemistry enabled low-temperature synthesis of lithium fluoride coatings for durable lithium anodes, ACS Appl. Mater. Interfaces 10 (2018) 26972–26981, https://doi.org/10.1021/acsami.8b04573.

[43] C. Ban, S.M. George, Molecular layer deposition for surface modification of lithium-ion battery electrodes, Adv. Mater. Interfaces. 3 (2016) 1600762, https://doi.org/10.1002/admi.201600762.

[44] L. Chen, Z. Huang, R. Shahbazian-Yassar, J.A. Libera, K.C. Klavetter, K.R. Zavadil, J.W. Elam, Directly formed alucone on lithium metal for high-performance Li batteries and Li-S batteries with high sulfur mass loading, ACS Appl. Mater. Interfaces 10 (2018) 7043–7051, https://doi.org/10.1021/acsami.7b15879.

[45] Y. Sun, Y. Zhao, J. Wang, J. Liang, C. Wang, Q. Sun, X. Lin, K.R. Adair, J. Luo, D. Wang, R. Li, M. Cai, T.-K. Sham, X. Sun, A novel organic “polyurea” thin film for ultralong-life lithium-metal anodes via molecular-layer deposition, Adv. Mater. (2018) 1806541, https://doi.org/10.1002/adma.201806541.

[46] L. Wang, Q. Wang, W. Jia, S. Chen, P. Gao, J. Li, Li metal coated with amorphous Li3PO4via magnetron sputtering for stable and long-cycle life lithium metal batteries, J. Power Sources 342 (2017) 175–182, https://doi.org/10.1016/j.jpowsour.2016.11.097.

[47] L. Wang, L. Zhang, Q. Wang, W. Li, B. Wu, W. Jia, Y. Wang, J. Li, H. Li, Long lifespan lithium metal anodes enabled by Al2O3 sputter coating, Energy Storage Mater. 10 (2018) 16–23, https://doi.org/10.1016/j.ensm.2017.08.001.

[48] E. Cha, M.D. Patel, J. Park, J. Hwang, V. Prasad, K. Cho, W. Choi, 2D MoS2as an efficient protective layer for lithium metal anodes in high-performance Li-S

batteries, Nat. Nanotechnol. 13 (2018) 337–343, https://doi.org/10.1038/s41565-018-0061-y.
[49] X. Wang, M. Zhang, J. Alvarado, S. Wang, M. Sina, B. Lu, J. Bouwer, W. Xu, J. Xiao, J.G. Zhang, J. Liu, Y.S. Meng, New insights on the structure of electrochemically deposited lithium metal and its solid electrolyte interphases via cryogenic TEM, Nano Lett. 17 (2017) 7606–7612, https://doi.org/10.1021/acs.nanolett.7b03606.
[50] D.B. Hall, P. Underhill, J.M. Torkelson, Spin coating of thin and ultrathin polymer films, Polym. Eng. Sci. 38 (1998) 2039–2045, https://doi.org/10.1002/pen.10373.
[51] N.F. Himma, A.K. Wardani, I.G. Wenten, Preparation of superhydrophobic polypropylene membrane using dip-coating method: the effects of solution and process parameters, Polym. Plast. Technol. Eng. 56 (2017) 184–194, https://doi.org/10.1080/03602559.2016.1185666.
[52] U. Siemann, Solvent cast technology – a versatile tool for thin film production, in: N. Stribeck, B. Smarsly (Eds.), Scatt. Methods Prop. Polym. Mater., Springer Berlin Heidelberg, Berlin, Heidelberg, 2005, pp. 1–14, https://doi.org/10.1007/b107336.
[53] Y. Gao, Y. Zhao, Y.C. Li, Q. Huang, T.E. Mallouk, D. Wang, Interfacial chemistry regulation via a skin-grafting strategy enables high-performance lithium-metal batteries, J. Am. Chem. Soc. 139 (2017) 15288–15291, https://doi.org/10.1021/jacs.7b06437.
[54] K. Liu, A. Pei, H.R. Lee, B. Kong, N. Liu, D. Lin, Y. Liu, C. Liu, P. chun Hsu, Z. Bao, Y. Cui, Lithium metal anodes with an adaptive "solid-liquid" interfacial protective layer, J. Am. Chem. Soc. 139 (2017) 4815–4820, https://doi.org/10.1021/jacs.6b13314.
[55] W. Liu, W. Li, D. Zhuo, G. Zheng, Z. Lu, K. Liu, Y. Cui, Core-shell nanoparticle coating as an interfacial layer for dendrite-free lithium metal anodes, ACS Cent. Sci. 3 (2017) 135–140, https://doi.org/10.1021/acscentsci.6b00389.
[56] F. Aziz, A.F. Ismail, Spray coating methods for polymer solar cells fabrication: a review, Mater. Sci. Semicond. Process. 39 (2015) 416–425, https://doi.org/10.1016/j.mssp.2015.05.019.
[57] M. Bai, K. Xie, K. Yuan, K. Zhang, N. Li, C. Shen, Y. Lai, R. Vajtai, P. Ajayan, B. Wei, A scalable approach to dendrite-free lithium anodes via spontaneous reduction of spray-coated graphene oxide layers, Adv. Mater. 30 (2018) 1801213, https://doi.org/10.1002/adma.201801213.
[58] H. Chen, A. Pei, D. Lin, J. Xie, A. Yang, J. Xu, K. Lin, J. Wang, H. Wang, F. Shi, D. Boyle, Y. Cui, Uniform high ionic conducting lithium sulfide protection layer for stable lithium metal anode, Adv. Energy Mater. 9 (2019) 1900858, https://doi.org/10.1002/aenm.201900858.
[59] D. Lin, Y. Liu, W. Chen, G. Zhou, K. Liu, B. Dunn, Y. Cui, Conformal lithium fluoride protection layer on three-dimensional lithium by nonhazardous gaseous reagent freon, Nano Lett. 17 (2017) 3731–3737, https://doi.org/10.1021/acs.nanolett.7b01020.
[60] J. Zhao, L. Liao, F. Shi, T. Lei, G. Chen, A. Pei, J. Sun, K. Yan, G. Zhou, J. Xie, C. Liu, Y. Li, Z. Liang, Z. Bao, Y. Cui, Surface fluorination of reactive battery anode materials for enhanced stability, J. Am. Chem. Soc. 139 (2017) 11550–11558, https://doi.org/10.1021/jacs.7b05251.
[61] F. Liu, Q. Xiao, H. Bin Wu, L. Shen, D. Xu, M. Cai, Y. Lu, Fabrication of hybrid silicate coatings by a simple vapor deposition method for lithium metal anodes, Adv. Energy Mater. 8 (2018) 1701744, https://doi.org/10.1002/aenm.201701744.
[62] J. Lang, Y. Long, J. Qu, X. Luo, H. Wei, K. Huang, H. Zhang, L. Qi, Q. Zhang, Z. Li, H. Wu, One-pot solution coating of high quality LiF layer to stabilize Li metal anode, Energy Storage Mater. 16 (2019) 85–90, https://doi.org/10.1016/j.ensm.2018.04.024.
[63] Z. Hu, S. Zhang, S. Dong, W. Li, H. Li, G. Cui, L. Chen, Poly(ethyl α-cyanoacrylate)-Based artificial solid electrolyte interphase layer for enhanced interface stability of Li metal anodes, Chem. Mater. 29 (2017) 4682–4689, https://doi.org/10.1021/acs.chemmater.7b00091.
[64] Q. Pang, X. Liang, A. Shyamsunder, L.F. Nazar, An in vivo formed solid electrolyte surface layer enables stable plating of Li metal, Joule 1 (2017) 871–886, https://doi.org/10.1016/j.joule.2017.11.009.
[65] A.M. Tripathi, W.N. Su, B.J. Hwang, In situ analytical techniques for battery interface analysis, Chem. Soc. Rev. 47 (2018) 736–751, https://doi.org/10.1039/c7cs00180k.
[66] R. Xu, X.Q. Zhang, X.B. Cheng, H.J. Peng, C.Z. Zhao, C. Yan, J.Q. Huang, Artificial soft–rigid protective layer for dendrite-free lithium metal anode, Adv. Funct. Mater. 28 (2018) 1705838, https://doi.org/10.1002/adfm.201705838.
[67] J. Luo, C.C. Fang, N.L. Wu, High polarity poly(vinylidene difluoride) thin coating for dendrite-free and high-performance lithium metal anodes, Adv. Energy Mater. 8 (2018) 1701482, https://doi.org/10.1002/aenm.201701482.
[68] N. Saqib, C.M. Ganim, A.E. Shelton, J.M. Porter, On the decomposition of carbonate-based lithium-ion battery electrolytes studied using operando infrared spectroscopy, J. Electrochem. Soc. 165 (2018) A4051–A4057, https://doi.org/10.1149/2.1051816jes.
[69] H. Liu, X. Yue, X. Xing, Q. Yan, J. Huang, V. Petrova, H. Zhou, P. Liu, A scalable 3D lithium metal anode, Energy Storage Mater. 16 (2019) 505–511, https://doi.org/10.1016/j.ensm.2018.09.021.
[70] H. Zheng, D. Xiao, X. Li, Y. Liu, Y. Wu, J. Wang, K. Jiang, C. Chen, L. Gu, X. Wei, Y.S. Hu, Q. Chen, H. Li, New insight in understanding oxygen reduction and evolution in solid-state lithium-oxygen batteries using an in situ environmental scanning electron microscope, Nano Lett. 14 (2014) 4245–4249, https://doi.org/10.1021/nl500862u.
[71] Y. Li, Y. Li, A. Pei, K. Yan, Y. Sun, C.L. Wu, L.M. Joubert, R. Chin, A.L. Koh, Y. Yu, J. Perrino, B. Butz, S. Chu, Y. Cui, Atomic structure of sensitive battery materials and interfaces revealed by cryo–electron microscopy, Science 358 (2017) 506–510, https://doi.org/10.1126/science.aam6014 (80-.).
[72] X. Wang, Y. Li, Y.S. Meng, Cryogenic electron microscopy for characterizing and diagnosing batteries, Joule 2 (2018) 2225–2234, https://doi.org/10.1016/j.joule.2018.10.005.
[73] M.J. Zachman, Z. Tu, S. Choudhury, L.A. Archer, L.F. Kourkoutis, Cryo-STEM mapping of solid–liquid interfaces and dendrites in lithium-metal batteries, Nature 560 (2018) 345–349, https://doi.org/10.1038/s41586-018-0397-3.
[74] H. Liu, X. Wang, H. Zhou, H.D. Lim, X. Xing, Q. Yan, Y.S. Meng, P. Liu, Structure and solution dynamics of lithium methyl carbonate as a protective layer for lithium metal, ACS Appl. Energy Mater. 1 (2018) 1864–1869, https://doi.org/10.1021/acsaem.8b00348.
[75] L. Lin, F. Liang, K. Zhang, H. Mao, J. Yang, Y. Qian, Lithium phosphide/lithium chloride coating on lithium for advanced lithium metal anode, J. Mater. Chem. A. 6 (2018) 15859–15867, https://doi.org/10.1039/c8ta05102j.
[76] L. Chen, J.G. Connell, A. Nie, Z. Huang, K.R. Zavadil, K.C. Klavetter, Y. Yuan, S. Sharifi-Asl, R. Shahbazian-Yassar, J.A. Libera, A.U. Mane, J.W. Elam, Lithium metal protected by atomic layer deposition metal oxide for high performance anodes, J. Mater. Chem. A. 5 (2017) 12297–12309, https://doi.org/10.1039/c7ta03116e.
[77] T. Liu, L. Lin, X. Bi, L. Tian, K. Yang, J. Liu, M. Li, Z. Chen, J. Lu, K. Amine, K. Xu, F. Pan, In situ quantification of interphasial chemistry in Li-ion battery, Nat. Nanotechnol. 14 (2019) 50–56, https://doi.org/10.1038/s41565-018-0284-y.
[78] B.D. Adams, J. Zheng, X. Ren, W. Xu, J.G. Zhang, Accurate determination of coulombic efficiency for lithium metal anodes and lithium metal batteries, Adv. Energy Mater. 8 (2018) 1702097, https://doi.org/10.1002/aenm.201702097.
[79] Y. Xu, T. Li, L. Wang, Y. Kang, Interlayered dendrite-free lithium plating for high-performance lithium-metal batteries, Adv. Mater. 37 (2019) 1901662, https://doi.org/10.1002/adma.201901662.
[80] X. Fan, L. Chen, O. Borodin, X. Ji, J. Chen, S. Hou, T. Deng, J. Zheng, C. Yang, S. C. Liou, K. Amine, K. Xu, C. Wang, Non-flammable electrolyte enables li-metal batteries with aggressive cathode chemistries, Nat. Nanotechnol. 13 (2018) 715–722, https://doi.org/10.1038/s41565-018-0183-2.
[81] A. Sakuda, A. Hayashi, M. Tatsumisago, Sulfide solid electrolyte with favorable mechanical property for all-solid-state lithium battery, Sci. Rep. 3 (2013) 2261, https://doi.org/10.1038/srep02261.
[82] H. Yildirim, A. Kinaci, M.K.Y. Chan, J.P. Greeley, First-Principles analysis of defect thermodynamics and ion transport in inorganic SEI compounds: LiF and NaF, ACS Appl. Mater. Interfaces 7 (2015) 18985–18996, https://doi.org/10.1021/acsami.5b02904.
[83] S. Hao, C. Wolverton, Lithium transport in amorphous Al2O3 and AlF 3 for discovery of battery coatings, J. Phys. Chem. C 117 (2013) 8009–8013, https://doi.org/10.1021/jp311982d.
[84] X. Yu, J.B. Bates, G.E. Jellison, F.X. Hart, A stable thin-film lithium electrolyte: lithium phosphorus oxynitride, J. Electrochem. Soc. 144 (1997) 524–532, https://doi.org/10.1149/1.1837443.
[85] G. Nazri, Preparation, structure and ionic conductivity of lithium phosphide, Solid State Ion. 34 (1989) 97–102, https://doi.org/10.1016/0167-2738(89)90438-4.
[86] M. Prencipe, A. Zupan, R. Dovesi, E. Aprà, V.R. Saunders, Ab initio study of the structural properties of LiF, NaF, KF, LiCl, NaCl, and KCl, Phys. Rev. B. 51 (1995) 3391–3396, https://doi.org/10.1103/PhysRevB.51.3391.
[87] R.M. SPRIGGS, L.A. BRISSETTE, Expressions for shear modulus and Poisson's ratio of porous refractory oxides, J. Am. Ceram. Soc. 45 (1962) 198–199, https://doi.org/10.1111/j.1151-2916.1962.tb11121.x.
[88] E.G. Herbert, W.E. Tenhaeff, N.J. Dudney, G.M. Pharr, Mechanical characterization of LiPON films using nanoindentation, Thin Solid Films 520 (2011) 413–418, https://doi.org/10.1016/j.tsf.2011.07.068.
[89] A. Sakuda, A. Hayashi, Y. Takigawa, K. Higashi, M. Tatsumisago, Evaluation of elastic modulus of Li2S-P2S5glassy solid electrolyte by ultrasonic sound velocity measurement and compression test, J. Ceram. Soc. Japan. 121 (2013) 946–949, https://doi.org/10.2109/jcersj2.121.946.
[90] H. Peelaers, C.G. Van De Walle, Elastic constants and pressure-induced effects in MoS2, J. Phys. Chem. C 118 (2014) 12073–12076, https://doi.org/10.1021/jp503683h.
[91] R.R. Nair, W. Ren, R. Jalil, I. Riaz, V.G. Kravets, L. Britnell, P. Blake, F. Schedin, A.S. Mayorov, S. Yuan, M.I. Katsnelson, H.M. Cheng, W. Strupinski, L. G. Bulusheva, A.V. Okotrub, I.V. Grigorieva, A.N. Grigorenko, K.S. Novoselov, A. K. Geim, Fluorographene: a two-dimensional counterpart of Teflon, Small 6 (2010) 2877–2884, https://doi.org/10.1002/smll.201001555.
[92] A.C. Kozen, C.F. Lin, O. Zhao, S.B. Lee, G.W. Rubloff, M. Noked, Stabilization of lithium metal anodes by hybrid artificial solid electrolyte interphase, Chem. Mater. 29 (2017) 6298–6307, https://doi.org/10.1021/acs.chemmater.7b01496.
[93] X. Liang, Q. Pang, I.R. Kochetkov, M.S. Sempere, H. Huang, X. Sun, L.F. Nazar, A facile surface chemistry route to a stabilized lithium metal anode, Nat. Energy. 2 (2017) 17119, https://doi.org/10.1038/nenergy.2017.119.
[94] X. Shen, Y. Li, T. Qian, J. Liu, J. Zhou, C. Yan, J.B. Goodenough, Lithium anode stable in air for low-cost fabrication of a dendrite-free lithium battery, Nat. Commun. 10 (2019) 900, https://doi.org/10.1038/s41467-019-08767-0.
[95] S. Chen, J. Zheng, L. Yu, X. Ren, M.H. Engelhard, C. Niu, H. Lee, W. Xu, J. Xiao, J. Liu, J.G. Zhang, High-efficiency lithium metal batteries with fire-retardant electrolytes, Joule 2 (2018) 1548–1558, https://doi.org/10.1016/j.joule.2018.05.002.
[96] X. Fan, X. Ji, F. Han, J. Yue, J. Chen, L. Chen, T. Deng, J. Jiang, C. Wang, Fluorinated solid electrolyte interphase enables highly reversible solid-state Li metal battery, Sci. Adv. 4 (2018), eaau9245.

[97] S. Jiao, X. Ren, R. Cao, M.H. Engelhard, Y. Liu, D. Hu, D. Mei, J. Zheng, W. Zhao, Q. Li, N. Liu, B.D. Adams, C. Ma, J. Liu, J.G. Zhang, W. Xu, Stable cycling of high-voltage lithium metal batteries in ether electrolytes, Nat. Energy. (2018) 1–8, https://doi.org/10.1038/s41560-018-0199-8.

[98] N.D. Trinh, D. Lepage, D. Aymé-Perrot, A. Badia, M. Dollé, D. Rochefort, An artificial lithium protective layer that enables the use of acetonitrile-based electrolytes in lithium metal batteries, Angew. Chem. Int. Ed. 57 (2018) 5072–5075, https://doi.org/10.1002/anie.201801737.

[99] J. Pan, Y.T. Cheng, Y. Qi, General method to predict voltage-dependent ionic conduction in a solid electrolyte coating on electrodes, Phys. Rev. B. 91 (2015) 134116, https://doi.org/10.1103/PhysRevB.91.134116.

[100] C. Li, L. Gu, J. Maier, Enhancement of the Li conductivity in LiF by introducing glass/crystal interfaces, Adv. Funct. Mater. 22 (2012) 1145–1149, https://doi.org/10.1002/adfm.201101798.

[101] J. Yang, C. Hu, Y. Jia, Y. Pang, L. Wang, W. Liu, X. Sun, Surface restraint synthesis of an organic-inorganic hybrid layer for dendrite-free lithium metal anode, ACS Appl. Mater. Interfaces 11 (2019) 8717–8724, https://doi.org/10.1021/acsami.9b00507.

[102] S.T. Myung, K. Izumi, S. Komaba, Y.K. Sun, H. Yashiro, N. Kumagai, Role of alumina coating on Li-Ni-Co-Mn-O particles as positive electrode material for lithium-ion batteries, Chem. Mater. 17 (2005) 3695–3704, https://doi.org/10.1021/cm050566s.

[103] S. Mo, B. Zhang, K. Zhang, S. Li, F. Pan, LiAl 5 O 8 as a potential coating material in lithium-ion batteries: a first principles study, Phys. Chem. Chem. Phys. 21 (2019) 13758–13765, https://doi.org/10.1039/c9cp02650a.

[104] X. Han, Y. Gong, K. Fu, X. He, G.T. Hitz, J. Dai, A. Pearse, B. Liu, H. Wang, G. Rubloff, Y. Mo, V. Thangadurai, E.D. Wachsman, L. Hu, Negating interfacial impedance in garnet-based solid-state Li metal batteries, Nat. Mater. 16 (2017) 572–579, https://doi.org/10.1038/nmat4821.

[105] Y. Shen, Y. Zhang, S. Han, J. Wang, Z. Peng, L. Chen, Unlocking the energy capabilities of lithium metal electrode with solid-state electrolytes, Joule 2 (2018) 1674–1689, https://doi.org/10.1016/j.joule.2018.06.021.

[106] D.M. Seo, D. Chalasani, B.S. Parimalam, R. Kadam, M. Nie, B.L. Lucht, Reduction reactions of carbonate solvents for lithium ion batteries, ECS Electrochem. Lett. 3 (2014) A91–A93, https://doi.org/10.1149/2.0021409eel.

[107] H. Liu, H. Zhou, B.S. Lee, X. Xing, M. Gonzalez, P. Liu, Suppressing lithium dendrite growth with a single-component coating, ACS Appl. Mater. Interfaces 9 (2017) 30635–30642, https://doi.org/10.1021/acsami.7b08198.

[108] H. Liu, X. Wang, H. Zhou, H.-D. Lim, X. Xing, Q. Yan, Y.S. Meng, P. Liu, Structure and solution dynamics of lithium methyl carbonate as a protective layer for lithium metal, ACS Appl. Energy Mater. 1 (2018) 1864–1869, https://doi.org/10.1021/acsaem.8b00348.

[109] H. Zhou, H. Liu, Y. Li, X. Yue, X. Wang, M. Gonzalez, Y.S. Meng, P. Liu, In situ formed polymer gel electrolytes for lithium batteries with inherent thermal shutdown safety features, J. Mater. Chem. A. 7 (2019) 16984–16991, https://doi.org/10.1039/C9TA02341K.

[110] Y. Han, X. Duan, Y. Li, L. Huang, D. Zhu, Y. Chen, Effects of sulfur loading on the corrosion behaviors of metal lithium anode in lithium-sulfur batteries, Mater. Res. Bull. 68 (2015) 160–165, https://doi.org/10.1016/j.materresbull.2015.03.042.

[111] W. Liu, R. Guo, B. Zhan, B. Shi, Y. Li, H. Pei, Y. Wang, W. Shi, Z. Fu, J. Xie, Artificial solid electrolyte interphase layer for lithium metal anode in high-energy lithium secondary pouch cells, ACS Appl. Energy Mater. 1 (2018) 1674–1679, https://doi.org/10.1021/acsaem.8b00132.

[112] J. Lau, R.H. DeBlock, D.M. Butts, D.S. Ashby, C.S. Choi, B.S. Dunn, Sulfide solid electrolytes for lithium battery applications, Adv. Energy Mater. 8 (2018) 1800933, https://doi.org/10.1002/aenm.201800933.

[113] H.D. Lim, H.K. Lim, X. Xing, B.S. Lee, H. Liu, C. Coaty, H. Kim, P. Liu, Solid electrolyte layers by solution deposition, Adv. Mater. Interfaces. 5 (2018) 1701328, https://doi.org/10.1002/admi.201701328.

[114] J. Liang, X. Li, Y. Zhao, L.V. Goncharova, G. Wang, K.R. Adair, C. Wang, R. Li, Y. Zhu, Y. Qian, L. Zhang, R. Yang, S. Lu, X. Sun, In situ Li 3 PS 4 solid-state electrolyte protection layers for superior long-life and high-rate lithium-metal anodes, Adv. Mater. 30 (2018) 1804684, https://doi.org/10.1002/adma.201804684.

[115] Z. Jiang, L. Jin, Z. Han, W. Hu, Z. Zeng, Y. Sun, J. Xie, Facile generation of polymer-alloy hybrid layer towards dendrite-free lithium metal anode with improved moisture stability, Angew. Chem. Int. Ed. 58 (2019) 11374–11378, https://doi.org/10.1002/anie.201905712.

[116] C. Yan, X.B. Cheng, Y.X. Yao, X. Shen, B.Q. Li, W.J. Li, R. Zhang, J.Q. Huang, H. Li, Q. Zhang, An armored mixed conductor interphase on a dendrite-free lithium-metal anode, Adv. Mater. 30 (2018) 1804461, https://doi.org/10.1002/adma.201804461.

[117] K. Yan, H.W. Lee, T. Gao, G. Zheng, H. Yao, H. Wang, Z. Lu, Y. Zhou, Z. Liang, Z. Liu, S. Chu, Y. Cui, Ultrathin two-dimensional atomic crystals as stable interfacial layer for improvement of lithium metal anode, Nano Lett. 14 (2014) 6016–6022, https://doi.org/10.1021/nl503125u.

[118] H. Zhang, X. Liao, Y. Guan, Y. Xiang, M. Li, W. Zhang, X. Zhu, H. Ming, L. Lu, J. Qiu, Y. Huang, G. Cao, Y. Yang, L. Mai, Y. Zhao, H. Zhang, Lithiophilic-lithiophobic gradient interfacial layer for a highly stable lithium metal anode, Nat. Commun. 9 (2018) 3729, https://doi.org/10.1038/s41467-018-06126-z.

[119] J. Song, H. Lee, M.J. Choo, J.K. Park, H.T. Kim, Ionomer-liquid electrolyte hybrid ionic conductor for high cycling stability of lithium metal electrodes, Sci. Rep. 5 (2015) 14458, https://doi.org/10.1038/srep14458.

[120] A.F.M. Barton, Handbook of Solubility Parameters and Other Cohesion Parameters, second ed., 1991, https://doi.org/10.1002/9781119403647.ch305.

[121] A.F.M. Barton, Handbook of Polymer-Liquid Interaction Parameters and Solubility Parameters, first ed., CRC Press, 1990.

[122] B. Zhu, Y. Jin, X. Hu, Q. Zheng, S. Zhang, Q. Wang, J. Zhu, Poly (dimethylsiloxane) thin film as a stable interfacial layer for high-performance lithium-metal battery anodes, Adv. Mater. 29 (2017) 1603755, https://doi.org/10.1002/adma.201603755.

[123] I.S. Kang, Y.-S. Lee, D.-W. Kim, Improved cycling stability of lithium electrodes in rechargeable lithium batteries, J. Electrochem. Soc. 161 (2014) A53–A57, https://doi.org/10.1149/2.029401jes.

[124] J. Bae, Y. Qian, Y. Li, X. Zhou, J.B. Goodenough, G. Yu, Polar polymer–solvent interaction derived favorable interphase for stable lithium metal batteries, Energy Environ. Sci. (2019), https://doi.org/10.1039/c9ee02558h. Advance Article.

[125] U. Eduok, O. Faye, J. Szpunar, Recent developments and applications of protective silicone coatings: a review of PDMS functional materials, Prog. Org. Coat. 111 (2017) 124–163, https://doi.org/10.1016/j.porgcoat.2017.05.012.

[126] X. Xing, Y. Li, X. Wang, V. Petrova, H. Liu, P. Liu, Cathode electrolyte interface enabling stable Li–S batteries, Energy Storage Mater. 21 (2019) 474–480, https://doi.org/10.1016/j.ensm.2019.06.022.

[127] Q. Li, F.L. Zeng, Y.P. Guan, Z.Q. Jin, Y.Q. Huang, M. Yao, W.K. Wang, A.B. Wang, Poly (dimethylsiloxane) modified lithium anode for enhanced performance of lithium-sulfur batteries, Energy Storage Mater. 13 (2018) 151–159, https://doi.org/10.1016/j.ensm.2018.01.002.

[128] C.H. Tsao, P.L. Kuo, Poly(dimethylsiloxane) hybrid gel polymer electrolytes of a porous structure for lithium ion battery, J. Membr. Sci. 489 (2015) 36–42, https://doi.org/10.1016/j.memsci.2015.03.087.

[129] G. Zheng, C. Wang, A. Pei, J. Lopez, F. Shi, Z. Chen, A.D. Sendek, H.W. Lee, Z. Lu, H. Schneider, M.M. Safont-Sempere, S. Chu, Z. Bao, Y. Cui, High-performance lithium metal negative electrode with a soft and flowable polymer coating, ACS Energy Lett 1 (2016) 1247–1255, https://doi.org/10.1021/acsenergylett.6b00456.

[130] Q. Pang, L. Zhou, L.F. Nazar, Elastic and Li-ion–percolating hybrid membrane stabilizes Li metal plating, Proc. Natl. Acad. Sci. 115 (2018) 12389–12394, https://doi.org/10.1073/pnas.1809187115.

[131] V.A. Ganesh, A.S. Nair, H.K. Raut, T.T. Yuan Tan, C. He, S. Ramakrishna, J. Xu, Superhydrophobic fluorinated POSS-PVDF-HFP nanocomposite coating on glass by electrospinning, J. Mater. Chem. 22 (2012) 18479–18485, https://doi.org/10.1039/c2jm33088a.

[132] J.H. Kim, H.S. Woo, W.K. Kim, K.H. Ryu, D.W. Kim, Improved cycling performance of lithium-oxygen cells by use of a lithium electrode protected with conductive polymer and aluminum fluoride, ACS Appl. Mater. Interfaces 8 (2016) 32300–32306, https://doi.org/10.1021/acsami.6b10419.

[133] R.S. Yeo, Dual cohesive energy densities of perfluorosulphonic acid (Nafion) membrane, Polymer 21 (1980) 432–435, https://doi.org/10.1016/0032-3861(80)90015-4.

[134] J. Lopez, A. Pei, J.Y. Oh, G.-J.N. Wang, Y. Cui, Z. Bao, Effects of polymer coatings on electrodeposited lithium metal, J. Am. Chem. Soc. 140 (2018) 11735–11744, https://doi.org/10.1021/jacs.8b06047.

[135] F. Qiu, X. Li, H. Deng, D. Wang, X. Mu, P. He, H. Zhou, A concentrated ternary-salts electrolyte for high reversible Li metal battery with slight excess Li, Adv. Energy Mater. 9 (2019) 1803372, https://doi.org/10.1002/aenm.201803372.

[136] T.T. Beyene, H.K. Bezabh, M.A. Weret, T.M. Hagos, C.-J. Huang, C.-H. Wang, W.-N. Su, H. Dai, B.-J. Hwang, Concentrated dual-salt electrolyte to stabilize Li metal and increase cycle life of anode free Li-metal batteries, J. Electrochem. Soc. 166 (2019) A1501–A1509, https://doi.org/10.1149/2.0731908jes.

[137] X. Cao, X. Ren, L. Zou, M.H. Engelhard, W. Huang, H. Wang, B.E. Matthews, H. Lee, C. Niu, B.W. Arey, Y. Cui, C. Wang, J. Xiao, J. Liu, W. Xu, J.-G. Zhang, Monolithic solid–electrolyte interphases formed in fluorinated orthoformate-based electrolytes minimize Li depletion and pulverization, Nat. Energy. 4 (2019) 796–805, https://doi.org/10.1038/s41560-019-0464-5.

[138] X. Zhang, A. Wang, X. Liu, J. Luo, Dendrites in lithium metal anodes: suppression, regulation, and elimination, Acc. Chem. Res. 52 (2019) 3223–3232, https://doi.org/10.1021/acs.accounts.9b00437.

[139] Y. Zhu, J. Xie, A. Pei, B. Liu, Y. Wu, D. Lin, J. Li, H. Wang, H. Chen, J. Xu, A. Yang, C.L. Wu, H. Wang, W. Chen, Y. Cui, Fast lithium growth and short circuit induced by localized-temperature hotspots in lithium batteries, Nat. Commun. 10 (2019) 2067, https://doi.org/10.1038/s41467-019-09924-1.